An inhibitor of Oxidative phosphorylation exploits cancer vulnerability

Jennifer R. Molina[1,2*], Yuting Sun[1,2*], Marina Protopopova[1,2], Sonal Gera[1,2], Madhavi Bandi[1,2], Christopher Bristow[1,2], Timothy McAfoos[1], Pietro Morlacchi[1,10], Jeffrey Ackroyd[11], Ahmed-Noor A. Agip[9], Gheath Al-Atrash[5], John Asara[13], Jennifer Bardenhagen[1], Caroline C Carrillo[6], Christopher Carroll[1], Edward Chang[1,2], Stefan Ciurea[5], Jason B. Cross[1], Barbara Czako[1], Angela Deem[1,2], Naval Daver[3], John Frederick de Groot[6], Jian-Wen Dong[6], Ningping Feng[1,2], Guang Gao[1,2], Jason Gay[1,2], Mary Geck Do[1], Jennifer Greer[1], Virginia Giuliani[1,2], Jing Han[1,2], Lina Han[3], Verlene K Henry[6], Judy Hirst[9], Sha Huang [1], Yongying Jiang[1], Zhijun Kang[1], Tin Khor[1,2], Sergej Konoplev[7], Yu-Hsi Lin[11], Gang Liu[1], Alessia Lodi[8], Timothy Lofton[1], Helen Ma[3], Mikhila Mahendra[1,2], Polina Matre[3], Robert Mullinax[1,2], Michael Peoples[1,2], Alessia Petrocchi[1], Jaime Rodriguez-Canale[12], Riccardo Serreli[9], Thomas Shi[1,2], Melinda Smith[1,2], Yoko Tabe[3,15], Jay Theroff[1], Stefano Tiziani[8], Quanyun Xu[1], Qi Zhang[3], Florian Muller[11], Ronald A. DePinho[14], Carlo Toniatti[1,2], Giulio F. Draetta[1,2,3], Timothy P. Heffernan[1,2], Marina Konopleva[3], Philip Jones[1,*], M. Emilia Di Francesco[1,*] and Joseph R. Marszalek[1,2,*,§]

[1] Institute for Applied Cancer Science, University of Texas MD Anderson Cancer Center, Houston, Texas 77030, USA.
[2] Center for Co-Clinical Trials, University of Texas MD Anderson Cancer Center, Houston, Texas 77030, USA.
[3]Department of Leukemia, University of Texas MD Anderson Cancer Center, Houston, Texas 77030, USA.
[4] Department of Genomic Medicine, University of Texas MD Anderson Cancer Center, Houston, Texas 77030, USA..
[5] Department of Stem Cell Transplantation and Cellular Therapy, University of Texas MD Anderson Cancer Center, Houston, Texas 77030, USA.
[6] Department of Neuro-Oncology, University of Texas MD Anderson Cancer Center, Houston, Texas 77030, USA.
[7] Department of Hematopathology, University of Texas MD Anderson Cancer Center, Houston, Texas 77030, USA.
[8] Department of Nutritional Sciences, The University of Texas at Austin, Austin, TX, USA
[9] Medical Research Council Mitochondrial Biology Unit, Wellcome Trust / MRC Building, Cambridge Biomedical Campus, Cambridge University, Hills Road, Cambridge, CB2 0XY, United Kingdom.
[10] Agilent Technologies Inc. 121 Hartwell Ave. Lexington, MA 02421.
[11] Department of Cancer Imaging Systems, University of Texas MD Anderson Cancer Center, Houston, Texas 77030, USA.
[12] Department of Translational Molecular Pathology, University of Texas MD Anderson Cancer Center, Houston, Texas 77030, USA.
[13] Beth Israel Deaconess Medical Center, Harvard Medical School, Boston, MA, USA
[14] Department of Cancer Biology, University of Texas MD Anderson Cancer Center, Houston, Texas 77030, USA
[15] Department of Next Generation Hematology Laboratory Medicine, Department of Laboratory Medicine, Juntendo University School of Medicine, Hongo 2-1-1,Bunkyo-ku, Tokyo Japan 113-8421.

* These authors contributed equally to this work.
§ Corresponding author

SUMMARY

Metabolic reprograming is an emerging hallmark of tumor biology and an actively pursued opportunity in oncology drug discovery. Extensive efforts have focused on therapeutic targeting of glycolysis, whereas drugging mitochondrial oxidative phosphorylation (OXPHOS) has remained largely unexplored, partly due to an incomplete understanding of tumor contexts where OXPHOS is essential. Here, we report the discovery of IACS-010759, a clinical-grade small-molecule inhibitor of complex I of the mitochondrial electron transport chain. Treatment with IACS-010759 robustly inhibited proliferation and induced apoptosis in models of brain cancer and acute myeloid leukemia (AML) reliant on OXPHOS, likely due to a combination of energy depletion and reduced aspartate production, leading to impaired nucleotide biosynthesis. IACS-010759 yielded potent tumor growth inhibition *in vivo* at well-tolerated doses in brain cancer and AML models and is currently being evaluated in Phase I clinical trials in relapsed/refractory AML and solid tumors.

Metabolic reprogramming is a well-appreciated hallmark of cancer, thus prompting extensive drug discovery activity in this area. Coordinated upregulation of glycolysis, known as the Warburg effect [1], is a phenomenon that arises as tumor cells adapt to increased demands for energy and biomass production. Elevated glycolysis is currently being exploited clinically using FDG-PET to detect metabolically active tumors [2], as well as therapeutically through the development of inhibitors of enzymes essential for glucose metabolism [3]. Recent reports emphasize that, in addition to a strong dependence on glycolysis, many tumors or cancer cell subpopulations rely on OXPHOS [4] for bioenergetic [5-15] and biosynthetic processes [16,17]. Biguanides, such as metformin, have been evaluated for the treatment of diabetes and metabolic disorders, providing rationale that targeting OXPHOS for clinical benefit can be done safely. However, metformin and other drugs targeting oxidative metabolism possess pharmacological limitations, including inadequate potency (i.e., biguanides) [18,19], transport-mediated accumulation (i.e., OCT1 for metformin) [20], off-target pharmacology (i.e., rotenone) [21], or lack of a suitable pharmacokinetic (PK) profile (i.e., oligomycin), which will restrict their use as oncology therapeutics. Here, we report the discovery of IACS-010759 (Fig. 1a), a clinical-grade, highly potent and selective small-molecule inhibitor of complex I of the mitochondrial electron transport chain (ETC; Fig. 1b) and its mechanism of anti-tumor activity in acute myeloid leukemia (AML) and genetically defined subsets of glioblastoma/neuroblastoma.

IACS-010759 was identified through an extensive medicinal chemistry campaign of lead optimization initially seeded with known modulators of HIF1α that act via inhibition of OXPHOS [22-24]. Consistent with IACS-010759 acting solely at complex I, treatment of detergent-permeabilized cells with IACS-010759 in medium supplemented with pyruvate/malate (to generate NADH for use by complex I) resulted in attenuated oxygen consumption rate (OCR;

Fig. 1c), whereas OCR was not affected by treatment with IACS-010759 when medium was supplemented with succinate to feed complex II, thus bypassing the requirement for complex I function. The mechanism was further supported by the finding that ectopic expression of *Saccharomyces cerevisiae* NDI1, the yeast complex I ortholog [25,26], completely restored cell viability and OCR to baseline levels in the presence of IACS-010759 (Fig. 1d and Supplementary Fig. 1a,b). Similar results were obtained with rotenone, a well-established but less-specific complex I inhibitor (Supplementary Fig. 1c), although only a partial rescue of viability was observed, likely due to off-target toxicity (Supplementary Figs. 2b,d,g,i,j,l). Further, IACS-010759 treatment of complex I isolated from mouse mitochondria resulted in decreased catalysis due to inhibition at the ubiquinone-binding site versus the flavin site, with no effect on H_2O_2 generation (Fig. 1e). To define the interaction of IACS-010759 with complex I, clones with reduced sensitivity to IACS-010759 were generated by growing cells for 12 weeks in the presence of increasing amounts of IACS-010759 in galactose medium, wherein cells were rendered dependent on OXPHOS for survival [27,28]. IC_{50} values for resistant clones ranged from 3.7-74 nM, compared to 1.1 nM for parental cells (Supplementary Fig. 1d). In contrast, sensitivity to rotenone was minimally changed in most clones (Supplementary Fig. 1d), indicating that the reduced sensitivity was unlikely due to a general decrease in complex I dependence (see Fig. 1f for representative dose response curves for clone DC4 and parental cell line). Total and mitochondrial RNA from 12 clones was subjected to next-generation sequencing, which confirmed that nine of the clones contained an identical nucleotide change in their mitochondrial DNA (mtDNA; C3469T) yielding an L55F amino acid substitution in the ND1 subunit of complex I (Fig. 1g). This residue resides close to the entrance of the proposed ubiquinone-10 binding channel of complex 1 (Figs. 1h,i) [29], but numerous attempts to ectopically

express mutant ND1-L55F utilizing multiple strategies were unsuccessful due to the technical challenges of ectopically expressing proteins encoded by mtDNA. Taken together, these data are consistent with IACS-010759 binding in or at the entrance to the ubiquinone channel, thus blocking ubiquinone binding or function to inhibit complex I activity.

To correlate the phenotypic response directly with OXPHOS inhibition, the effect of IACS-010759 on OCR of cells grown in Seahorse medium was compared to the viability of cells grown in galactose-containing medium. IACS-010759 robustly inhibited both OCR and galactose-dependent cell viability, producing nearly identical IC_{50} values of 1.4 nM for both assays (Fig. 1j). By comparison, rotenone treatment resulted in OCR and galactose-dependent cell viability IC_{50} values of 0.24 nM and 0.87 nM, respectively (Supplementary Fig. 1e). IC_{50} values were similar across several human cell line models for both compounds (Supplemental Table I). To inform on the potency of IACS-010759 across widely used preclinical safety species, the response of representative cell lines from mouse, rat, dog, and cynomolgus monkey were assessed using the highly quantitative galactose growth assay. IACS-010759 was similarly active in mouse (Avg. IC_{50} = 5.6 nM), rat (IC_{50} = 12.2 nM) and cynomolgus monkey (IC_{50}= 8.7 nM), thus making them appropriate preclinical models for further safety studies (Supplemental Table I). In contrast, IACS-010759 was minimally active in canine cell lines (IC_{50} 180 nM to 360 nM). Rotenone potency was very similar across all species (Supplemental Table I).

The effect of IACS-010759 on cell growth and viability was evaluated across a panel of cancer cell lines and normal diploid cells standard culture medium containing IACS-010759, which provides multiple energy sources to the cells. IACS-010759 yielded a >50% maximal reduction in growth in the majority of cancer cell lines (24/30 pancreatic (PDAC), 19/20 ovarian, 13/16 triple-negative breast (TNBC), 8/10 non-small cell lung (NSCLC)), while a subset (11/30 PDAC,

10/20 ovarian, 5/16 TNBC and 2/10 NSCLC) exhibited >100% growth inhibition (Supplementary Fig. 3a-d). All diploid cell lines were insensitive to IACS-010759 with little or no growth inhibition (Supplementary Fig. 2a,c,g,i,k), whereas rotenone exposure reduced viability in these models, consistent with rotenone possessing non-specific "off-target" toxicities (Supplementary Fig. 2b,d,h,j,l). These data establish differential sensitivity of normal and cancer cells to OXPHOS inhibition by IACS-010759.

In addition to direct anti-growth effects, OXPHOS inhibition has been reported to reduce hypoxia and HIF pathway activity [4,22,24,30]. Consistently, exposure of cell line spheres to IACS-010759 eliminated hypoxia, most likely as a consequence of increased intracellular oxygen (Supplementary Fig. 4a,b). This coincided with decreased HIF pathway activity (Supplementary Fig. 4c) via oxygen-, prolyl hydroxylase- and VHL-dependent degradation of HIF1α (Supplementary Figs. 4d-h).

IACS-010759 targets glycolysis-deficient tumor cells

Glycolysis is under negative control by OXPHOS and is induced by tricarboxylic acid cycle (TCA)-mediated allosteric inhibition of glyocolytic enzymes (the "Pasteur effect" [31]); therefore, genetic or pharmacological OXPHOS inhibition should result in compensatory upregulation of glycolysis to maintain ATP levels and redox balance, resulting in modest anti-proliferation effects [32]. We thus hypothesized that tumor cells with reduced capacity for compensatory glycolysis would be more sensitive to OXPHOS inhibition.

As previously reported, a subpopulation of brain tumor cell lines with homozygous deletion of Enolase 1 (*ENO1*) are glycolysis deficient due to a >90% reduction of cellular enolase enzymatic activity [33,34]. Consistent with glycolysis inhibition at enolase, the levels of glycolysis metabolites

upstream of enolase were elevated in *ENO1*-null cell lines, such as D423 and Gli56, while metabolites downstream of enolase were reduced relative to glioblastoma multiforme (GBM) cell lines heterozygous or wild-type for *ENO1* (Supplementary Fig. 5a). Ectopic expression of wild-type ENO1 in Gli56 and D423 (Supplementary Fig. 5b) robustly increased lactate production, consistent with restoration of glycolysis (Fig. 2a and Supplementary Fig. 5c). Further, there was minimal lactate production upon treatment of parental Gli56 cells with IACS-010759, whereas the baseline and induction of lactate production were substantially increased in Gli56 cells ectopically expressing ENO1 (Supplementary Fig. 5d). Similar to ENO1-null cells, phosphoglycerate dehydrogenase (PGD)-null cells, such as the NB1 cell line, are glycolysis deficient, as these cells accumulate 6-phosphogluconate, an allosteric inhibitor of glucose-6-phosphate isomerase [35,36,37]. We evaluated the metabolic profile of NB1 cells by determining the ECAR:OCR ratio (Fig. 2b), and observed both an extremely low glycolysis:OXPHOS ratio and restored lactate production following ectopic expression of PGD (Fig. 2a). Furthermore, IACS-010759 treatment resulted in >70% reduction in viability and a 2- to 5-fold increase in apoptosis in NB-1, GLI56, or D423 cells, while ectopic expression of either ENO1 or PGD (Fig. 2c,d and Supplementary Figs. 6a-c) substantially attenuated the response. Similarly, the viability of *ENO1*$^{-/-}$ or *ENO1*$^{+/-}$ glioma sphere-derived cell lines was reduced upon IACS-010759 exposure (Supplementary Fig. 6d-f). These data are consistent with our hypothesis that glycolysis deficiency renders cell lines highly sensitive to OXPHOS inhibitors such as IACS-010759.

AML tumor cells are sensitive to IACS-010759

Previous reports have suggested that leukemia cells are highly OXPHOS dependent [6,7,11-13,38-40], warranting evaluation of IACS-010759 in AML models. Established AML cell lines were exposed to a range of IACS-010759 concentrations for 3 to 7 days, resulting in reduced viability

with EC_{50} values of <3 nM (Fig. 2e and Supplementary Fig. 7a). While the inflection point of response (EC_{50}) was equivalent across cell lines (Supplementary Fig. 7a), the effect on viability varied, with MOLM-13 (FLT3-ITD mutated) being relatively insensitive (Fig. 2e). Treatment with IACS-010759 uniformly reduced OCR, indicating that the differential effects on viability are not due to lack of OXPHOS inhibition, consistent with our finding of similar EC_{50} values across cell lines (Supplementary Fig. 7b). In most cell lines, IACS-010759 treatment modestly increased apoptosis by up to 2-fold (Fig. 2h). Cells responded more robustly to IACS-010759 treatment when glucose availability was restricted, whereas glutamine restriction did not enhance the response (Supplementary Fig. 7c,d), consistent with glucose utilization being the primary compensatory response to OXPHOS inhibition. Interestingly, MOLM-13 had the highest baseline OCR and largest glycolytic reserve of the cell lines evaluated, both of which may contribute to its relative insensitivity to IACS-010759 (Supplementary Fig. 7b). This might represent a potential mechanism for treatment resistance and is consistent with results reported for OXPHOS inhibition in melanoma models [41]. We extended our studies to primary AML blasts isolated from peripheral blood of relapsed/refractory patients by treating blasts *ex vivo* with multiple concentrations of IACS-010759 for up to 5 days. In nearly all primary AML samples, but not in non-transformed mononuclear cells isolated from normal bone marrow, IACS-010759 reduced viability and induced apoptosis (Fig. 2f,g,i,j and Supplemental Table II), consistent with our observations in AML cell lines and supporting a therapeutic window for IACS-010759 to selectively target leukemic versus normal hematopoietic cells. The patient-derived xenograft (PDX-4030094), also responded robustly to IACS-010759 (approximate IC_{50} <1.5 nM) upon *ex vivo* treatment (Supplementary Fig. 7e). Further, we evaluated IACS-010759 response in cell lines established from two previously described murine AML models genetically engineered to

196 ectopically co-express the clinically relevant translocation *MLL/ENL* in a *KRAS*^{G12D} background
197 with or without *TP53* deletion [42]. Viability and OCR were inhibited equally in both cell lines
198 (Supplementary Fig. 7f,g) with approximate IC_{50} values of 20 nM and 55 nM, respectively.
199 These results, taken together with those in ENO1- and PGD-null GBM models, define two
200 biological tumor contexts with striking sensitivity to IACS-010759.

201 **IACS-010759 safely targets glycolysis-deficient tumors *in vivo***

202 To determine whether the observed *in vitro* and *ex vivo* effects predicted *in vivo* responses in
203 preclinical models at tolerated doses, we evaluated IACS-010759 in murine models of
204 glioblastoma/neuroblastoma and AML. The PK profile of IACS-010759 was determined in mice
205 following intravenous (0.3 mg/kg) and oral (1 mg/kg) administration (Supplementary Fig. 8a).
206 IACS-010759 was characterized by low plasma clearance with a high volume of distribution,
207 resulting in a prolonged terminal half-life (>24 hours) with sustained levels of plasma exposure
208 following oral dosing. Conversion of IACS-010759 free base into the corresponding HCl salt
209 resulted in a ~10-fold increase in plasmatic exposure after oral dosing (Supplementary Fig. 8b).
210 Consistent with previous reports for metformin[43], we did not observe changes in blood glucose
211 level with single or repeated doses of IACS-010759 (Supplementary Fig. 8c). However, at 2
212 hours post a first or fifth dose, plasma insulin levels transiently decreased, returning to control
213 levels by 24 hours post-dose (Supplementary Fig. 8d).

214 To assess the tolerability and anti-tumor activity of IACS-010759 in a glycolysis-deficient
215 context, mice bearing NB-1 (PGD-null) subcutaneous xenografts received daily oral doses of 0,
216 5, 10, or 25 mg/kg/day free base IACS-010759 for 21 days. Treatment with 5 or 10 mg/kg IACS-
217 010759 resulted in tumor regression with minimal body weight loss (Fig. 3a and Supplementary

Fig. 8e), whereas IACS-010759 25 mg/kg was not tolerated, with observations of body weight loss (Supplementary Fig. 8e), lethargy, and hypothermia. At the tolerated doses, IACS-010759 was equally effective and well tolerated with various intermittent dosing schedules (Supplementary Fig. 8f,g), providing flexibility for dosing. Transient, intermittent treatment of Gli56 intracranial tumors with 5 mg/kg IACS-010759.HCl using a 5 day on/2 day off schedule for 4 weeks reduced tumor size as measured by MRI (Figs. 3b,c) and extended median survival from 84 days to 130 days (Supplementary Fig. 9a). Tumor hypoxia was eliminated in Gli56 and D423 intracranial tumors after two daily doses of IACS-010759.HCl 5 mg/kg (Supplementary Fig. 9b,c) compared to vehicle control-treated animals, supporting OXPHOS inhibition within the tumor. We also observed 84% and 43% reductions in the number of cells positive for the mitotic marker phospho-histone H3 in IACS-010759.HCl-treated Gli56 and D423 tumors, respectively, compared to control-treated animals (Supplementary Fig. 9d-g), which is indicative of reduced tumor cell proliferation. Collectively these data provide evidence of profound anti-tumor activity of IACS-010759 at well-tolerated doses in the context of glycolysis-deficient brain tumors.

Immunohistochemistry (IHC) analysis of tumor samples from 92 patients treated at The University of Texas MD Anderson Cancer Center was conducted to determine the prevalence of ENO1- and PGD-null GBM toward defining a potential clinical path. Eight tumors (8.6%) were either unambiguously ENO1-negative (3.3%) or showed very low ENO1 staining (5 tumors (5.3%)), which represented a slightly higher percentage of ENO1-deficient tumors compared to reports from The Cancer Genome Atlas (TCGA) sequencing data (Fig. 3d and Supplementary Fig. 9h). Whether tumors with weak staining represent non-specific background or very low expression of ENO1 could not be ascertained and will require independent validation with

orthogonal assays. Regardless, a clinically relevant population of at least 3% was clearly identified. It should be noted that the strong, residual signal represents ENO1 expression in non-tumor stromal cells, such as microglia, lymphoid cells, and blood vessel endothelial and smooth muscle cells (Supplementary Fig. 9i,j and 10a-d). No tumors PGD-null tumors were identified. Based on this analysis, we conclude that ENO1-depleted GBM tumors can be detected and therefore represent a viable, clinically relevant population expected to benefit from treatment with IACS-010759.

IACS-010759 is tolerated and extends survival in murine models of AML

In vivo AML models were evaluated to confirm the anti-tumor activity and tolerability of IACS-010759 in this context. The OCI-AML3 cell line, PDX-4030094 (*MLL*-rearranged AML PDX model refractory to standard-of-care treatment), PDX-S6-AP (PDX with complex cytogenetics and unfavorable prognosis), and three genetically defined murine leukemia syngeneic models[42] were grown orthotopically in mice. Seven days after inoculation with OCI-AML3 cells, mice were dosed orally for 35 days with 10 mg/kg IACS-010759.HCl or vehicle using several intermittent schedules (Fig. 3e) and doses that were all well tolerated (Supplementary Fig. 11a, 11c). Daily dosing schedules (QD or 5 on/2 off) were most effective and increased median survival from 28 days to longer than 60 days, while less-frequent dosing schedules (Q2D or Q3D) enhanced survival to a lesser extent (Fig. 3e). In the PDX-4030094 model, IACS-010759.HCl 2.5 or 7.5 mg/kg/day nearly doubled median survival from 35 days to almost 70 days (Fig. 3f and Supplementary Fig. 11b), while IACS-010759.HCl 1 mg/kg/day extended survival to 55 days. Additionally, disease burden, as measured by splenic hCD45 abundance at treatment day 21, was significantly reduced in IACS-010759-treated groups relative to vehicle-

treated groups (Supplementary Fig. 11d). IACS-10759 similarly improved survival in the PDX-S6-AP model (Supplementary Fig. 11e). Treatment of the highly aggressive, matched-pair *MLL/ENL* translocation syngeneic models with IACS-010759 resulted in modest but statistically significantly prolonged survival in the *TP53*$^{-/-}$, but not the *TP53*$^{+/+}$ model (Supplementary Fig. 11f,g). In contrast, the murine syngeneic model, AML1/ETO9a (KRAS^{G12D}, p53-null), was more sensitive to IACS-010759, with significant decreases in disease burden at days 8 (42%) and 15 (24%) (Supplementary Fig. 11h) and statistically significantly extended median survival from 17 days to 21 days (24%) (Supplementary Fig. 11i). Similarly to the xenograft models, all three syngeneic models experienced transient loss of body weight during the first week of dosing (Supplementary Fig. 11j-l). Overall, the consistent anti-leukemia responses observed *in vitro* and *in vivo* provided the preclinical rationale to evaluate IACS-010759 in a phase 1 study in subjects with relapsed/refractory AML (NCT02882321), which enrolled its first subject in October 2016.

OXPHOS inhibition leads to depletion of energy and nucleotide biosynthesis

To better understand the molecular mechanism by which IACS-010759 exerts anti-tumor activity, we performed metabolomic analyses, stable-isotope tracing experiments, and functional characterization on a subset of AML cell lines. IACS-l010759 induced modest increases in ROS levels, consistent with previous reports examining OXPHOS inhibition[41,44] (Supplementary Fig. 12a). To evaluate metabolic reprogramming, OCI-AML3 cells were exposed to IACS-010759 for 6, 24, or 72 hours, and the resultant cell lysates were subjected to LC/MS analysis to measure metabolites from central carbon metabolism and amino acids. IACS-010759 treatment elevated the intracellular steady-state level of the complex I substrate, NADH, as well as nucleotide monophophates (NMPs), while reducing nucleotide triphophates (NTPs), all consistent with

285 complex I inhibition and reduced energetic status (Fig. 4a). This was further confirmed by
286 elevated p^{T172}-AMPK levels (see Fig. 4j, Supplementary Fig. 12m), a well-established readout of
287 energetic stress. Stable isotope-tracing experiments using uniformly labelled ^{13}C-glucose (Fig.
288 4b) revealed that IACS-010759 significantly increased incorporation of ^{13}C-glucose into the
289 glycolysis endpoints lactate and alanine, as evaluated by m+3 isotopologue fractions (Fig. 4c),
290 and decreased incorporation into TCA intermediates and mitochondria-produced metabolites
291 (m+2 isotopologue fractions), including aspartate and glutamate (Fig. 4d), suggesting that
292 glucose utilization through these pathways was significantly reduced. Although IACS-010759-
293 treated cells uptake less glutamine compared to control cells (Supplementary Fig. 12b), tracing
294 experiments with uniformly labeled ^{13}C-glutamine confirmed that treatment with IACS-010759
295 increased incorporation of ^{13}C-glutamine carbons into the TCA cycle to fuel both oxidative and
296 reductive metabolism, likely to support fatty acid biosynthesis, but failed to productively
297 contribute toward aspartate synthesis (Supplementary Fig. 12c-f) [45]. These observations suggest
298 an increased utilization of glutamine as an alternative compensatory mechanism to IACS-010759
299 treatment.

300 Targeted metabolomics in OCI-AML3 cells showed that, consistent with other published
301 findings [16,17]. To assess whether aspartate was incorporated into nucleotides, as has been
302 suggested [16,17], OCI-AML3 cells were grown with uniformly labelled ^{13}C-aspartate. After
303 treatment with IACS-010759, an increased m+3 isotopologue fraction of several nucleotides was
304 observed (Fig. 4f,g) that was consistent with increased utilization of exogenous aspartate for
305 nucleotide biosynthesis, which suggests that mitochondria-produced aspartate becomes rate
306 limiting upon OXPHOS inhibition. While aspartate supplementation partially restored cell
307 growth (Fig. 4h, Supplementary Fig. 12g,h), cell cycle progression, and incorporation of BrdU

into cycling cells (Fig. 4i, Supplementary Fig. 12i), it failed to influence p^{T172}-AMPK activation, indicating persistent energetic stress (Fig. 4j, Supplementary Fig. 12m). Interestingly, AMPK activation does not appear to be essential for the reduced tumor cell viability observed upon IACS-010759 exposure, as shRNA-mediated knockdown of AMPK in OCI-AML3 cells minimally impacted cell viability (Supplementary Fig. 12j,k). Aspartate also abrogated IACS-010759-induced accumulation of DNA damage, as measured by p^{S139}-γH2AX (Fig. 4j). Interestingly, aspartate supplementation was not able to rescue the proliferation phenotype in the relatively insensitive MOLM-13 cell line, suggesting that the hypersensitive cell lines may rely on OXPHOS for energy as well as aspartate production (Supplementary Fig. 12h). As an additional response mechanism, we found that IACS-010759 markedly increased expression of the CD14 myeloid differentiation marker in OCI-AML3 cells (Supplementary Fig. 12l), but not in MOLM-13 cells (data not shown). Taken together, we propose that IACS-010759-mediated reduction in cell viability and induction of differentiation or apoptosis result from a combination of energy depletion and reduced aspartate production (Fig. 5a,b).

Therapeutic targeting of OXPHOS in AML

Based on mechanisms defined by *in vitro* studies, we evaluated the effects of IACS-010759 on OCR, aspartate, proliferation, and differentiation status in blast cells from PDX-4030094 *in vivo*. Blast cells were harvested from mouse spleens 2 hours after the first dose or 24 hours after a second dose of IACS-010759.HCl (representing C_{max} and C_{trough}, respectively; Fig. 5b). At each dose and time point, OCR, aspartate, and an IACS-010759-regulated transcriptomic signature (Supplementary Fig. 13a-f) were measured to establish a relationship among PK, pharmacodynamic (PD), and efficacy outcomes. At 2 hours, OCR was equally inhibited at all

doses (Fig. 5c, Supplementary Fig. 14a). By 48 hours, OCR (Fig. 5d, Supplementary Fig. 14b), aspartate (Fig. 5f) and the gene expression signature (Fig. 5g) were suppressed in a dose-dependent manner at the 2.5- and 7.5-mg doses, which correlated with increased survival (see Fig. 3f). At both time points, aspartate levels were unaltered at 1 mg/kg but suppressed in a dose-dependent manner at the top two doses (Fig. 5e,f), suggesting that aspartate level is a less-sensitive measure than OCR or the gene expression signature. Blasts isolated from animals that received two doses of IACS-010759 (7.5 mg/kg) exhibited reduced proliferation (Fig. 5h) and increased apoptosis (Fig. 5i). Additionally, IACS-010759 treatment reduced the fraction of $CD34^+$ stem/progenitor AML cells (Fig. 5j) in a dose-dependent manner, most likely due to induction of leukemia cell differentiation, as suggested by enrichment of AML cells expressing the myeloid differentiation antigens, MNDA, CD14, CD11b, and CD68 (Fig. 5k and Supplementary Fig. 15a-k). These data support employing OCR, aspartate levels, gene expression changes, and markers of differentiation as PD biomarkers to assess the biology of response in clinical samples from patients with relapsed/refractory AML treated with OXPHOS inhibitors such as IACS-010759.

Advancing IACS-010759 into clinical evaluation

The anti-tumor activity of IACS-010759 in glycolysis-deficient GBM/neuroblastoma tumors and relapsed/refractory AML justified evaluation of IACS-010759 in clinical studies. During preclinical development, we evaluated IACS-010759 PK in mouse, rat, dog, and cynomolgus monkey, which indicated that the compound displayed low clearance, large volume of distribution, and long terminal half-life (Supplementary Table III). In a battery of *in vitro* studies, IACS-010759 did not show any significant effects in binding assays on a panel of 80 receptors

and ion channels (Supplemental Table IV), nor did IACS-010759 inhibit the hERG K^+ channel current (IC_{50} >30 μM) (Supplementary Fig. 16) or modulate CYP enzyme activity (data not shown). In *in vivo* toxicity studies that included dose-range finding, acute intravenous dosing, repeated oral dosing (both daily and intermittent), and a pivotal GLP-compliant 28-day oral toxicity study with a 28-day recovery period in the Sprague-Dawley rat and cynomolgus monkey, drug-related adverse events included emesis and decreased body weight at lower doses. At the highest doses, decreased core body temperature and death were observed, consistent with anticipated effects of excessive OXPHOS inhibition. No-observed-adverse-effect dose levels (NOAELs) were identified in rat and monkey that supported the ability for oral daily doses to yield plasma drug concentrations above those anticipated to result in on-target drug effects. These data were used to establish the human starting dose per FDA guidelines [46].

Our findings contrast with the century-old tenet, put forth in Otto Warburg's seminal work, that glycolysis is the dominant metabolic pathway to which tumors become addicted[1]. In recent years, the field has dispelled the notion that the increased glycolysis observed in tumors is simply a mechanism to provide additional energy to support the high rate of proliferation, and instead has indicated that the adaptation serves to provide macromolecule building blocks for biosynthetic processes that are critical for enhanced tumor growth. Through the development and characterization IACS-010759, we now provide evidence that clinically translatable contexts exist where tumors are highly dependent on OXPHOS for survival. We further demonstrate that subsets of tumors depend on OXPHOS not only for ATP synthesis, but also to produce macromolecules necessary for biosynthetic processes, similar to glycolysis. In the most sensitive tumor cells, OXPHOS disruption creates an environment of energy and macromolecule depletion that leads to cell cycle arrest, apoptosis, and, in the case of AML, differentiation, similar to what

has been reported with small-molecule inhibitors of mutant IDH [47]. Taken together, our preclinical data support clinical evaluation of IACS-010759 in AML and solid tumors that lack compensatory glycolytic capacity. First-in-human clinical studies with IACS-010759 are ongoing in patients with AML and solid tumors to establish proof-of-concept, define the maximum tolerated dose, and provide initial verification of the hypotheses generated by this work.

REFERENCES

1 Warburg, O., Wind, F. & Negelein, E. The Metabolism of Tumors in the Body. *J Gen Physiol* **8**, 519-530 (1927).

2 Palaskas, N. *et al.* 18F-fluorodeoxy-glucose positron emission tomography marks MYC-overexpressing human basal-like breast cancers. *Cancer Res* **71**, 5164-5174, doi:10.1158/0008-5472.CAN-10-4633 (2011).

3 DeBerardinis, R. J. & Chandel, N. S. Fundamentals of cancer metabolism. *Sci Adv* **2**, e1600200, doi:10.1126/sciadv.1600200 (2016).

4 Koppenol, W. H., Bounds, P. L. & Dang, C. V. Otto Warburg's contributions to current concepts of cancer metabolism. *Nat Rev Cancer* **11**, 325-337, doi:10.1038/nrc3038 (2011).

5 Caro, P. *et al.* Metabolic signatures uncover distinct targets in molecular subsets of diffuse large B cell lymphoma. *Cancer Cell* **22**, 547-560, doi:10.1016/j.ccr.2012.08.014 S1535-6108(12)00356-X [pii] (2012).

6 Goto, M. *et al.* Importance of glutamine metabolism in leukemia cells by energy production through TCA cycle and by redox homeostasis. *Cancer Invest* **32**, 241-247, doi:10.3109/07357907.2014.907419 (2014).

7 Goto, M. *et al.* Adaptation of leukemia cells to hypoxic condition through switching the energy metabolism or avoiding the oxidative stress. *BMC Cancer* **14**, 76, doi:10.1186/1471-2407-14-76 (2014).

8 Haq, R. *et al.* Oncogenic BRAF regulates oxidative metabolism via PGC1alpha and MITF. *Cancer Cell* **23**, 302-315, doi:10.1016/j.ccr.2013.02.003 S1535-6108(13)00067-6 [pii] (2013).

9 Hu, J. *et al.* Heterogeneity of tumor-induced gene expression changes in the human metabolic network. *Nat Biotechnol* **31**, 522-529, doi:10.1038/nbt.2530 nbt.2530 [pii] (2013).

10 Roesch, A. *et al.* Overcoming Intrinsic Multidrug Resistance in Melanoma by Blocking the Mitochondrial Respiratory Chain of Slow-Cycling JARID1B(high) Cells. *Cancer Cell* **23**, 811-825, doi:10.1016/j.ccr.2013.05.003 S1535-6108(13)00196-7 [pii] (2013).

11 Simsek, T. *et al.* The distinct metabolic profile of hematopoietic stem cells reflects their location in a hypoxic niche. *Cell Stem Cell* **7**, 380-390, doi:10.1016/j.stem.2010.07.011 S1934-5909(10)00347-4 [pii] (2010).
12 Skrtic, M. *et al.* Inhibition of mitochondrial translation as a therapeutic strategy for human acute myeloid leukemia. *Cancer Cell* **20**, 674-688, doi:10.1016/j.ccr.2011.10.015 S1535-6108(11)00398-9 [pii] (2011).
13 Sriskanthadevan, S. *et al.* AML cells have low spare reserve capacity in their respiratory chain that renders them susceptible to oxidative metabolic stress. *Blood* **125**, 2120-2130, doi:10.1182/blood-2014-08-594408 (2015).
14 Vazquez, F. *et al.* PGC1alpha expression defines a subset of human melanoma tumors with increased mitochondrial capacity and resistance to oxidative stress. *Cancer Cell* **23**, 287-301, doi:10.1016/j.ccr.2012.11.020 S1535-6108(13)00034-2 [pii] (2013).
15 Viale, A. *et al.* Oncogene ablation-resistant pancreatic cancer cells depend on mitochondrial function. *Nature* **514**, 628-632, doi:10.1038/nature13611 (2014).
16 Birsoy, K. *et al.* An Essential Role of the Mitochondrial Electron Transport Chain in Cell Proliferation Is to Enable Aspartate Synthesis. *Cell* **162**, 540-551, doi:10.1016/j.cell.2015.07.016 (2015).
17 Sullivan, L. B. *et al.* Supporting Aspartate Biosynthesis Is an Essential Function of Respiration in Proliferating Cells. *Cell* **162**, 552-563, doi:10.1016/j.cell.2015.07.017 (2015).
18 Bridges, H. R., Jones, A. J., Pollak, M. N. & Hirst, J. Effects of metformin and other biguanides on oxidative phosphorylation in mitochondria. *Biochem J* **462**, 475-487, doi:10.1042/BJ20140620 (2014).
19 Dykens, J. A. *et al.* Biguanide-induced mitochondrial dysfunction yields increased lactate production and cytotoxicity of aerobically-poised HepG2 cells and human hepatocytes in vitro. *Toxicol Appl Pharmacol* **233**, 203-210, doi:10.1016/j.taap.2008.08.013 (2008).
20 Wang, D. S. *et al.* Involvement of organic cation transporter 1 in hepatic and intestinal distribution of metformin. *J Pharmacol Exp Ther* **302**, 510-515, doi:10.1124/jpet.102.034140 (2002).
21 Sanchez, M., Gastaldi, L., Remedi, M., Caceres, A. & Landa, C. Rotenone-induced toxicity is mediated by Rho-GTPases in hippocampal neurons. *Toxicol Sci* **104**, 352-361, doi:10.1093/toxsci/kfn092 (2008).
22 Ellinghaus, P. *et al.* BAY 87-2243, a highly potent and selective inhibitor of hypoxia-induced gene activation has antitumor activities by inhibition of mitochondrial complex I. *Cancer Med* **2**, 611-624, doi:10.1002/cam4.112 (2013).
23 Li, S. H. *et al.* A novel mode of action of YC-1 in HIF inhibition: stimulation of FIH-dependent p300 dissociation from HIF-1{alpha}. *Mol Cancer Ther* **7**, 3729-3738, doi:10.1158/1535-7163.MCT-08-0074 (2008).
24 Lin, X. *et al.* A chemical genomics screen highlights the essential role of mitochondria in HIF-1 regulation. *Proc Natl Acad Sci U S A* **105**, 174-179, doi:10.1073/pnas.0706585104 (2008).
25 Bai, Y. *et al.* Lack of complex I activity in human cells carrying a mutation in MtDNA-encoded ND4 subunit is corrected by the Saccharomyces cerevisiae NADH-quinone

oxidoreductase (NDI1) gene. *J Biol Chem* **276**, 38808-38813, doi:10.1074/jbc.M106363200

M106363200 [pii] (2001).

26 Seo, B. B. *et al.* Molecular remedy of complex I defects: rotenone-insensitive internal NADH-quinone oxidoreductase of Saccharomyces cerevisiae mitochondria restores the NADH oxidase activity of complex I-deficient mammalian cells. *Proc Natl Acad Sci U S A* **95**, 9167-9171 (1998).

27 Petrova-Benedict, R., Buncic, J. R., Wallace, D. C. & Robinson, B. H. Selective killing of cells with oxidative defects in galactose medium: a screening test for affected patient fibroblasts. *J Inherit Metab Dis* **15**, 943-944 (1992).

28 Robinson, B. H., Petrova-Benedict, R., Buncic, J. R. & Wallace, D. C. Nonviability of cells with oxidative defects in galactose medium: a screening test for affected patient fibroblasts. *Biochem Med Metab Biol* **48**, 122-126 (1992).

29 Zhu, J., Vinothkumar, K. R. & Hirst, J. Structure of mammalian respiratory complex I. *Nature* **536**, 354-358, doi:10.1038/nature19095 (2016).

30 Chang, E. *et al.* 18F-FAZA PET imaging response tracks the reoxygenation of tumors in mice upon treatment with the mitochondrial complex I inhibitor BAY 87-2243. *Clin Cancer Res* **21**, 335-346, doi:10.1158/1078-0432.CCR-14-0217

1078-0432.CCR-14-0217 [pii] (2015).

31 Krebs, H. A. The Pasteur effect and the relations between respiration and fermentation. *Essays Biochem* **8**, 1-34 (1972).

32 Hao, W., Chang, C. P., Tsao, C. C. & Xu, J. Oligomycin-induced bioenergetic adaptation in cancer cells with heterogeneous bioenergetic organization. *J Biol Chem* **285**, 12647-12654, doi:10.1074/jbc.M109.084194 (2010).

33 Leonard, P. G. *et al.* SF2312 is a natural phosphonate inhibitor of enolase. *Nat Chem Biol* **12**, 1053-1058, doi:10.1038/nchembio.2195 (2016).

34 Muller, F. L. *et al.* Passenger deletions generate therapeutic vulnerabilities in cancer. *Nature* **488**, 337-342, doi:10.1038/nature11331

nature11331 [pii] (2012).

35 Gaitonde, M. K., Murray, E. & Cunningham, V. J. Effect of 6-phosphogluconate on phosphoglucose isomerase in rat brain in vitro and in vivo. *J Neurochem* **52**, 1348-1352 (1989).

36 Jeffery, C. J., Hardre, R. & Salmon, L. Crystal structure of rabbit phosphoglucose isomerase complexed with 5-phospho-D-arabinonate identifies the role of Glu357 in catalysis. *Biochemistry* **40**, 1560-1566 (2001).

37 Sukhatme, V. P. & Chan, B. Glycolytic cancer cells lacking 6-phosphogluconate dehydrogenase metabolize glucose to induce senescence. *FEBS Lett* **586**, 2389-2395, doi:10.1016/j.febslet.2012.05.052 (2012).

38 Boultwood, J. *et al.* Amplification of mitochondrial DNA in acute myeloid leukaemia. *Br J Haematol* **95**, 426-431 (1996).

39 Lagadinou, E. D. *et al.* BCL-2 inhibition targets oxidative phosphorylation and selectively eradicates quiescent human leukemia stem cells. *Cell Stem Cell* **12**, 329-341, doi:10.1016/j.stem.2012.12.013

S1934-5909(12)00755-2 [pii] (2013).

40 Samudio, I. *et al.* Pharmacologic inhibition of fatty acid oxidation sensitizes human leukemia cells to apoptosis induction. *The Journal of clinical investigation* **120**, 142-156, doi:10.1172/JCI38942 (2010).
41 Schockel, L. *et al.* Targeting mitochondrial complex I using BAY 87-2243 reduces melanoma tumor growth. *Cancer Metab* **3**, 11, doi:10.1186/s40170-015-0138-0 (2015).
42 Zuber, J. *et al.* Mouse models of human AML accurately predict chemotherapy response. *Genes Dev* **23**, 877-889, doi:10.1101/gad.1771409 (2009).
43 Wheaton, W. W. *et al.* Metformin inhibits mitochondrial complex I of cancer cells to reduce tumorigenesis. *Elife* **3**, e02242, doi:10.7554/eLife.02242 (2014).
44 Sancho, P. *et al.* MYC/PGC-1alpha Balance Determines the Metabolic Phenotype and Plasticity of Pancreatic Cancer Stem Cells. *Cell Metab* **22**, 590-605, doi:10.1016/j.cmet.2015.08.015 (2015).
45 Griss, T. *et al.* Metformin Antagonizes Cancer Cell Proliferation by Suppressing Mitochondrial-Dependent Biosynthesis. *PLoS Biol* **13**, e1002309, doi:10.1371/journal.pbio.1002309 (2015).
46 FDA. Guidance for Industry - Estimating the Maximum Safe Starting Dose in Initial Clinical Trials for Therapeutics in Adult Healthy Volunteers;
47 Kernytsky, A. *et al.* IDH2 mutation-induced histone and DNA hypermethylation is progressively reversed by small-molecule inhibition. *Blood* **125**, 296-303, doi:10.1182/blood-2013-10-533604 (2015).

ACKNOWLEDGEMENTS

We thank members of the Center for Co-Clinical Trials, Institute for Applied Cancer Science, the GBM and AML/MDS Moon Shots for intellectual and financial support. We would especially like to express our gratitude and appreciation to Christopher Vellano for his help editing and assembling this manuscript. F. F. Lang and J. Gumin for providing GSC models; C. Kingsley and the MDACC Small Animals Imaging Facility; Nikunj Satani and Ellen Lin for validation of antibodies and preparation of samples for analysis. The Agilent Technologies Thought Leader Award for supporting P. Mo and R.A.D. A.-N.A.A., R.S., and J.Hi were supported by The Medical Research Council (U105663141). M.K., S.T., A.L., P.Ma., H.M. and Q.Z. were supported by CPRIT grant RP140218. F.L.M. was supported by the CPRIT RP140612, NIH CDP SPORE P50CA12700107, and ACS Research Scholar Grant RSG1514501CDD. G.F.D. was supported by the AACR 14-90-25 and by the Sheikh Ahmed Bin Zayed Al Nahyan Center for Pancreatic Cancer Grant. This work was supported in part by the MD Anderson Moon Shots program.

AUTHOR CONTRIBUTIONS

The studies designed with input from J.R.Ma., J.R.Mo., Y.S., M.Pr., C.B., P.Mo., J.Hi., M.K., P.J., M.E.D.F., C.T., T.P.H., G.F.D., F.M. and other authors. *In vitro* experiments were performed by J.R.Ma, J.R.Mo., V.G., L.Ha., Y. T., Y. S., M.Pr., S.G., M. M., T. K., M.B., P.Mo., J.B., G.G., M.G.D., J.Ha., Y.J., T.L., H.M., P.Ma., M.Pe., R.S., T.S., M.S., V.K.H., C.C.C. and Q.Z. IACS-010759 was developed and conceived by M.E.D., T.M., C.C., B.C., G.L., Z.K., A.P. and P.J. In vivo studies were performed by Y-H. L., N.F., J.Ga., J.Gr. and R.M. Immunohistochemistry was performed by J. A., E.C., S.K. and J.R-C. Computational chemistry was performed by J.Hu. and J.B.C. Pharmacokinetic analysis was performed by S.H., Q.X. and Y.J. FACS data analysis was performed by J.R.Mo. and S.G. Glioma Stem Cell work was performed by Y.S., T.S., J-W.D., V.K.H, J.F.d.G. and C.C.C. Bioinformatic analysis was performed by C.B. Clinical positioning in AML was designed by M.K., N.D., J.R.Ma, M.E.D and P.J. Metabolomic data for glycolysis deficient was generated by Y.S., C.B., and J.A., for leukemia by J.R.Mo., S.T., A.L., and P.Mo. Stable-isotope labeling study design, analysis and interpretation was performed by P. Mo. Mouse complex I assays were designed and performed by J.Hu., A.-N.A.A., and R. S. Normal bone marrow samples were provided by S.C. and G.A-A. Writing and preparation of the manuscript and figures were performed by J.R.Ma., J.R.Mo., T.P.H., R.A.D., A.D., Y.S., M.E.D.F., M.K., P. Mo. and P.J.

AUTHOR INFORMATION

The authors declare no competing financial interests.

Correspondence and requests for materials should be addressed to J.R.M. (JRMarszalek@mdanderson.org).

* These authors contributed equally to this work: Jennifer R. Molina, Yuting Sun, Philip Jones, M. Emilia Di Francesco, Joseph R. Marszalek

1. Institute for Applied Cancer Science, The University of Texas MD Anderson Cancer Center, Houston, Texas 77030, USA

Jennifer R. Molina, Yuting Sun, Marina Protopopova, Sonal Gera, Madhavi Bandi, Timothy McAfoos, Pietro Morlacchi, Jennifer Bardenhagen, Christopher Bristow, Guang Gao, John Asara, Christopher Carroll, Edward Chang, Jason Cross, Barbara Czako, Angela Deem, Ningping Feng, Jason Gay, Mary Geck Do, Virginia, Giuliani, Jennifer Greer, Jing Han, Sha Huang, Yongying Jiang, Zhijun Kang, Tin Khor, Gang Liu, Timothy Lofton, Mikhila Mahendra, Robert Mullinax, Michael Peoples, Alessia Petrocchi, Thomas Shi, Melinda Smith, Jay Theroff, Zuanyun Xu, Carlo Toniatti, Timothy P. Heffernan, Giulio F. Draetta, Philip Jones, M. Emila Di Francesco, Joseph R. Marszalek

2. Department of Leukemia, The University of Texas MD Anderson Cancer Center, Houston, Texas 77030, USA

Naval Daver, Lina Han, Helen Ma, Polina Matre, Yoko Tabe, Qi Zhang, Marina Konopleva

3. Department of Genomic Medicine, The University of Texas MD Anderson Cancer Center, Houston, Texas 77030, USA

Giulio F. Draetta

4. Department of Stem Cell Transplantation and Cellular Therapy, The University of Texas MD Anderson Cancer Center, Houston, Texas 77030, USA

Stefan Ciurea, Gheath Al-Atrash

5. Department of Neuro-Oncology, The University of Texas MD Anderson Cancer Center, Houston, Texas 77030, USA

Jian-Wen Dong, John Frederick de Groot, Verlene K Henry, Caroline C Carillo

6. Department of Hematopathology, The University of Texas MD Anderson Cancer Center, Houston, Texas 77030, USA

Sergej Konoplev

7. Department of Nutritional Sciences, The University of Texas at Austin, Austin, Texas 78712, USA

Alessia Lodi, Stefano Tiziani

8. Medical Research Council Mitochondrial Biology Unit, Wellcome Trust / MRC Building, Cambridge Biomedical Campus, Cambridge University, Hills Road, Cambridge, CB2 0XY, United Kingdom

Ahmed-Noor A. Agip, Judy Hirst, Riccardo Serreli

9. Agilent Technologies Inc. 121 Hartwell Ave. Lexington, MA 02421, USA

Pietro Morlacchi

10. Department of Cancer Imaging Systems, University of Texas MD Anderson Cancer Center, Houston, Texas 77030, USA

Florian Muller, Yu-His Lin, Jeffrey Ackroyd

11. Department of Translational Molecular Pathology, University of Texas MD Anderson Cancer Center, Houston, Texas 77030, USA.

Jaime Rodriguez-Canale

12. Beth Israel Deaconess Medical Center, Harvard Medical School, Boston, MA, USA

John Asara

13. Department of Cancer Biology, University of Texas MD Anderson Cancer Center, Houston, Texas 77030, USA

Ronald A. DePinho

14. Department of Next Generation Hematology Laboratory Medicine, Department of Laboratory Medicine, Juntendo University School of Medicine, Hongo 2-1-1,Bunkyo-ku, Tokyo Japan 113-8421.

Yoko Tabe

FIGURE LEGENDS

Figure 1. IACS-010759 is a potent inhibitor of mitochondria complex I. (a) Structure of IACS-010759. **(b)** Illustration of mitochondria electron transport chain. **(c)** OCR in permeabilized H460 cells grown in medium supplemented with pyruvate/malate to measure complex I activity, then treated with IACS-010759 (Injection I) and 10 mM succinate (Injection II) (n=2 cultures performed one time). **(d)** OCR in Seahorse medium (n=6 cultures, representative experiment out of 2 experiments) and relative viability (cell confluence) in galactose medium (n=2 cultures performed one time) were measured in H460 cells engineered to ectopically express *Saccharomyces cerevisiae* Ndi1 (complex I equivalent) or GFP following treatment with either DMSO or 14 nM IACS-010759 for 1 hour (OCR) or 72 hours (viability). **(e)** Complex I isolated from mouse mitochondria was treated with 60 nM IACS-010759 to measure effects on ubiquinone reduction (decylubiquinone) (n=9 technical replicates), flavin site activity via $APAD^+$ (n=3 technical replicates), and H_2O_2 production (n=3 technical replicates). **(f)** Dose-response for H292 clone resistant to IACS-010759 (n=2 cultures, performed one time). **(g)** Sanger sequencing chromatogram of PCR-amplified MT-ND1 DNA from an IACS-010759-resistant cell. **(h)** Structure of complex I showing location of ND1 subunit. **(i)** Location of L55F relative to the proposed ubiquinone binding channel (shown as a surface) in complex I. Residues and structures that form the binding site are shown; the redox-active ubiquinone headgroup moves through the channel and is reduced next to cluster N2. **(h)** and **(i)** were created using the highly homologous structure of bovine complex I (5LC5.pdb) [29]. **(j)** H460 cells were treated with IACS-010759 and OCR (n=6 cultures) and viability (n=2 cultures) were measured after 1 or 72 hours, respectively. ***p-value <0.0001 by two-sided student's t-test. c,d,j repeated once; e,f repeated ≥ 2 times, each with comparable results.

Figure 2. Glycolysis deficient and AML tumor cells are sensitive to OXPHOS inhibition.

(a) Extracellular lactate levels (glycolysis endpoint) in NB1 ($6PGD^{-/-}$), Gli56 ($ENO1^{-/-}$) and D423 ($ENO1^{-/-}$) cells and their counterparts each engineered to ectopically express either PGD (NB1) or ENO1 (Gli56 and D423) (Data represents the mean value of n=6 cultures for NB1 and D423 and n=3 cultures for Gli56). **(b)** Seahorse analysis measuring the ratio of glycolysis (proton production rate, PPR) to OXPHOS (OCR), (n=2 biological replicates). **(c)** Viability of same matched pair cell lines cultured in medium containing 100 nM IACS-010759 for 3 days (n=2 biological replicates for NB1 and D423; n=3 biological replicates for Gli56). **(d)** Percentage of annexin V-positive (+) NB1, Gli56, and D423 cells cultured in medium containing DMSO or 100 nM IACS-010759 for 3 days (n=3 cultures). **(e)** Viability of AML cell lines treated with indicated concentrations of IACS-010759 for 3 to 7 days (Data represents mean ± SD from n=3 cultures). **(f)** Viability of primary AML or **(g)** normal bone marrow samples treated *ex vivo* with 0, 10, 30 or 100 nM IACS-010759 for 4 or 5 days. IACS-010759-treated samples were normalized to corresponding DMSO-treated control. **(h)** Percentage of apoptotic cells (PI/annexin V) for each AML cell line (n=2 cultures, with replicate study performed only for OCI-AML3 with comparable results) after culturing for 72 hours in medium containing DMSO or 123 nM IACS-010759. **(i)** Percentage of apoptotic (annexin V positive) cells for primary AML or **(j)** normal bone marrow cells after culturing for 4 or 5 days in medium containing DMSO or IACS-010759. For f,g,i, and j, each point is the mean of 3 cultures from a single patient sample performed once; the bar for each concentration represents the mean value for all of the samples; patient sample (UPIN) characteristics are included in Supplementary Table II. p-

value ***<0.0001, **<0.001,*<0.05 by two-sided student's t-test. a-e, repeated one additional time with comparable results.

Figure 3. Glycolysis-deficient and AML xenografts are sensitive to OXPHOS inhibition. (a) Tumor volume of subcutaneous NB1 tumors in mice that received daily oral dosing of IACS-010759 or vehicle. (n=10 per group; data represents mean ± SEM). **(b,c)** Mice with ENO1-deficient Gli56 cells implanted intracranially were treated with vehicle or 5 mg/kg IACS-010759 for 4 weeks following a 5 on/2 off dosing schedule: **(b)** Representative pre- and post-treatment MRI coronal images of brain (vehicle n=5 mice, IACS-010759 n=7 mice; experiment repeated once with similar results). **(c)** Quantitation of tumor volumes calculated from MRI images at Day 33; (Box-whisker plots, min to max *p = 0.025 using two-sided Student's t-test). **(d)** Hematoxylin & eosin (H & E) and immunohistochemistry staining for 6PGD and ENO1 protein expression in GBM patient tumor array. Representative ENO1 wild-type (WT) and ENO1-null (-/-) tumors are shown. Scale bar = 100 μm. **(e)** Kaplan-Meier survival analysis of mice inoculated with OCI-AML3 cells and treated for 5 weeks (starting on Day 7) with oral vehicle or 10 mg/kg IACS-010759 daily (QD), 5 days on/ 2 days off (QDx5), every other day (Q2D), or every third day (Q3D). (n = 9 mice per group, p-values = 0.0007 [Q3D], 0.0008 [Q2D] and <0.0001 [QD and QDx5] by Mantel-Cox Log-rank test using GraphPad prism software) **(f)** Kaplan-Meier survival analysis of mice inoculated with primary patient sample 4030094 and treated with oral 1, 2.5, or 7.5 mg/kg IACS-010759 daily starting on Day 25. (n = 9 mice per group, p-values = 0.0002 [1 mg/kg] and <0.0001 [2.5 and 7.5 mg/kg] by Mantel-Cox Log-rank test using GraphPad prism software)

Figure 4. Inhibition of OXPHOS by IACS-010759 leads to energy deprivation and impairs nucleotide biosynthesis. (a) Targeted metabolomic analysis of nucleotide biomolecules in OCI-AML3 cells treated with 100 nM IACS-010759 for 6, 24, or 72 hr. The heatmap depicts alterations of metabolites associated with complex I and energy production as fold-change (log2) of treated versus DMSO control. p-values were derived using two-sided Welch's t-test accounting for unequal variance (n=4 cultures, mean, experiment repeated once with comparable results). **(b)** Illustration of [U-^{13}C]-glucose metabolism in OCI-AML3 cells. White circles = ^{12}C carbons; blue circles = ^{13}C carbons. Cells were grown in culture medium containing [U-^{13}C]-glucose and treated with DMSO or 100 nM IACS-010759 for 24 hours. **(c)** Incorporation of [U-^{13}C]-glucose into glycolysis endpoints [lactate (extracellular) and alanine (intracellular)], (n=4 cultures, mean plotted, p-value ***=0.0002, ****<0.0001 by two-sided Student's t-test.). **(d)** TCA intermediates (isocitrate, α-ketoglutarate, succinate and fumarate [intracellular]) and mitochondria metabolites (glutamate, glutathione and aspartate [intracellular]) in OCI-AML3 cells after treatment with DMSO or 100 nM IACS-010759 for 24 hours. (n=4 cultures, mean plotted, p-value ****<0.0001 by two-sided Student's t-test). **(e)** Targeted metabolomic analysis of amino acid biomolecules in OCI-AML3 cells treated with DMSO or 100 nM IACS-010759 for 6, 24, or 72 hours. The heatmap depicts alterations of as fold-change (log2) of treated versus DMSO control samples. p-values were derived using two-sided Welch's t-test accounting for unequal variance (; n=4 cultures, mean, experiment repeated once with comparable results). **(f)** Illustration of conversion of [U-^{13}C]-aspartate carbon into pyrimidines. Blue circles depict carbons derived from aspartate. **(g)** Incorporation of carbons derived from [U-^{13}C]-aspartate into representative pyrimidine metabolites in OCI-AML3 cells treated with DMSO or 100 nM IACS-010759 for 72 hours. (n=4 cultures, mean plotted, experiment repeated once with comparable

699 results). **(h)** OCI-AML3 cells were cultured in medium treated with DMSO, 100 nM IACS-
700 010759, or 100 nM IACS-010759 supplemented with 10 mM aspartate and the number of cells
701 was measured after 72 hours (n=2 cultures, experiment repeated once with comparable results).
702 **(i)** Incorporation of BrdU measured by flow cytometry in OCI-AML3 cells treated for 72 hours
703 with DMSO, 123 nM IACS-010759, or 123 nM IACS-010759 supplemented with 10 mM
704 aspartate. Cells were also stained with 7-AAD to detect DNA. **(j)** Immunoblot for activated
705 AMPK (p-AMPK, T172) and γ-H2AX (p-γ-H2AX, S139) in OCI-AML3 cells treated as
706 described. See supplementary figure 12m for blots with molecular weight markers. i,j repeated
707 once with comparable results.

708 **Figure 5. IACS-010759 modulates several clinically translatable pharmacodynamic**
709 **biomarkers (a)** Experimental workflow to assess pharmacokinetic and pharmacodynamic
710 relationship for mice inoculated with PDX-4030094 cells and treated with IACS-010759. **(b)**
711 Illustration schema for workflow to assess PD markers of target inhibition and biology of
712 response. After irradiation and inoculation, tumor burden was monitored. Upon 90% tumor
713 burden in the spleen (human CD45 versus mouse CD45), mice received 2 doses of IACS-010759
714 24 hours apart. Tumor cells were isolated from the spleen at 2 hours after the first dose or 24
715 hours after the second dose (2-hour (C_{max}) and 48-hour (C_{min}) time points, respectively). **(c)** OCR
716 of leukemia cells at the 2-hour and **(d)** 48-hour time points. **(e)** Aspartate levels of leukemia cells
717 at the 2-hour (FC = fold-change) and **(f)** 48-hour time points. **(g)** Change in expression of a 19-
718 gene (PD) score for leukemia cells at the 48-hour time point. **(h)** Average number of pHistone
719 H3-positive (+), **(i)** apoptotic cells measured by cleaved caspase 3, **(j)** CD34-positive (+), or **(k)**
720 MNDA-positive (+) cells per field in the spleen of mice treated with vehicle or IACS-010759 at
721 the 48–hour time point. c-g, each symbol represents the mean value for 3 technical replicates

722 from a single mouse.. h-k, each symbol is the mean of 5 random fields from a single mouse.
723 Mean ± SEM is provided. *p-value = 0.02, ***<0001, n.s. = not significant by two-sided student
724 t-test.

725

METHODS

Cell culture.

Unless otherwise specified, all cell lines (H460, 293T, H292, RCC4, RCC4+VHL, Gli56, D423 and NB-1) were cultured in DMEM (Gibco)+ 10%FBS (Sigma). AML cell lines (KG1, THP1, MOLM13, K562, MV4-11, OCI-AML3, U937, Kasumi, and HL60) were cultured in RPMI (Gibco) + 5%-20% FBS. D423 cells were provided by D. Bigner (Duncan et al, Oncotarget 2010). Gli56 cells were provided by D.N. Louis (Mueller et al, Oncogene 2005). NB-1 cells were obtained from JCRB Cell Bank. All GSCs were kindly provided by Dr. Fred Lang at MDACC. GSCs were cultured in serum-free DMEM/F12 (ATCC) supplemented with 20 ng/ml bFGF (Sigma) , 20 ng/ml EGF (Sigma) and 1x B27 supplement (Invitrogen). Normal diploid cells were purchased from ATCC and cultured following ATCC's guidelines. All other cell lines are from ATCC. RCC4 and RCC4VHL were obtained from ECACC. Cell lines are maintained by an internal core facility that routinely uses STR fingerprinting to verify cell line identity and mycoplasma testing to confirm they are negative.

Compound Synthesis

Step 1: Synthesis of ethyl 3-(4(trifluoromethoxy)phenyl)-1,2,4-oxadiazole-5-carboxylate

To a solution of (*E*)-*N'*-hydroxy-4-(trifluoromethoxy)benzimidamide (Sigma-Aldrich, 60.0 g, 272 mmol) and pyridine (32.3 g, 408 mmol) in $CHCl_3$ (400 mL) at 0 ^oC was slowly added ethyl 2-chloro-2-oxoacetate (44.6 g, 327 mmol). The mixture was stirred at reflux for 3 hrs, cooled to RT and diluted with H_2O (400 mL). The mixture was extracted with DCM (400 mL x2), the combined organic layers were washed with aq. HCl (1M, 300 mL x 2) and H_2O (400 mL), dried over Na_2SO_4, filtered, evaporated to give ethyl 3-(4(trifluoromethoxy)phenyl)-1,2,4-oxadiazole-5-carboxylate as a light yellow solid (77.7 g, 94%), which was used for next step without further purification. ^1H NMR (300 MHz, $CDCl_3$) δ 8.22 (d, *J*= 11.2 Hz, 2 H), 7.36 (d, *J*= 11.2 Hz, 2 H), 4.60 (q, *J*= 9.6 Hz, 2 H), 1.51 (t, *J*= 9.6 Hz, 3 H); ^{13}C NMR (126 MHz, DMSO-d_6) δ 167.5, 167.1, 153.5, 150.7, 129.5, 124.4, 121.7, 119.9 (q, J = 257 Hz), 63.3, 13.7; ^{19}F NMR (471 MHz, DMSO-d_6) δ -56.7; HRMS (ESI^+) m/z: $[M+H]^+$ calcd. for $C_{12}H_{10}F_3N_2O_4$ 303.0587; found 303.0584.

Step 2: Synthesis of 3-(4-(trifluoromethoxy)phenyl)-1,2,4-oxadiazole -5-carbohydrazide

To a solution of ethyl 3-(4-(trifluoromethoxy)phenyl)-1,2,4-oxadiazole-5-carboxylate (80.0 g, 265 mmol) in EtOH (800 mL) was added $NH_2NH_2.H_2O$ (85%, 76.0 mL, 1325 mmol). The reaction mixture was stirred at RT overnight. The desired compound precipitated from the reaction mixture, was filtered and washed with EtOH (200 mL) to afford 3-(4-(trifluoromethoxy)phenyl)-1,2,4-oxadiazole-5-carbohydrazide (70.2 g, 92%) as a light yellow solid, which was used for next step without further purification. ^1H NMR (600 MHz, Methanol-d_4) δ 8.24 (d, *J* = 8.8 Hz, 2H), 7.47 (d, *J* = 8.6 Hz, 2H); ^{13}C NMR (126 MHz, DMSO-d_6) δ 166.9, 129.4, 124.7, 121.7, 119.9 (q, J = 258 Hz); ^{19}F NMR (471 MHz, DMSO-d_6) δ -56.6; HRMS (ESI^+) m/z: $[M+H]^+$ calcd. for $C_{10}H_8F_3N_4O_3$ 289.0543; found 289.0538.

Step3: Synthesis of 5-(5-methyl-1H-1,2,4-triazol-3-yl)-3-(4-(trifluoromethoxy)phenyl)-1,2,4-oxadiazole

To a mixture of 3-(4-(trifluoromethoxy)phenyl)-1,2,4-oxadiazole-5-carbohydrazide (45.0 g, 156 mmol) and acetimidamide hydrochloride (22.2 g, 234 mmol) in THF (500 mL), was added NaOH (9.4 g, 234 mmol). The mixture was refluxed for 3 days and then cooled to RT, concentrated under reduced pressure and diluted with H_2O (500 mL). The resulting suspension was stirred at RT for 30 min, and then filtered to afford crude solid product, which was treated with EtOAc (400 mL). The resulting suspension was stirred at RT for 30 min, and then filtered to afford 5-(5-methyl-1H-1,2,4-triazol-3-yl)-3-(4-(trifluoromethoxy)phenyl)-1,2,4-oxadiazole as a white solid (30.3 g, 62%). ^{1}H NMR (600 MHz, DMSO-d_6) δ 14.65 (s, 1H), 8.22 (d, J = 8.7 Hz, 2H), 7.61 (d, J = 8.6 Hz, 2H), 2.51 (s, 3H); ^{13}C NMR (126 MHz, DMSO-d_6) δ 169.4, 167.2, 165.8, 155.3, 150.5, 129.4, 125.0, 121.7, 119.9 (q, J = 258 Hz), 11.5; ^{19}F NMR (471 MHz, DMSO-d_6) δ -56.6; HRMS (ESI$^+$) m/z: $[M+H]^+$ calcd. for $C_{12}H_9F_3N_5O_2$ 312.0703; found 312.0699.

Step 4: Synthesis of 5-(1-(3-bromobenzyl)-5-methyl-1H-1,2,4-triazol-3-yl)-3-(4-(trifluoromethoxy)phenyl)-1,2,4-oxadiazole

To a suspension of 5-(5-methyl-1H-1,2,4-triazol-3-yl)-3-(4-(trifluoromethoxy)phenyl) -1,2,4-oxadiazole (60.0 g, 192.8 mmol) and potassium carbonate (66.6 g, 482.0 mmol) in DMF (200 mL) was added 1-bromo-3-(bromomethyl)benzene (48.2 g, 192.8 mmol). The mixture was stirred at RT for 16h, then diluted with water (500 mL) and extracted with EtOAc (3 x 500 mL). The combined organic layers were washed with H_2O (300 mL) and concentrated under reduced pressure to afford the crude product, which was purified by silica gel chromatography column (eluent: 4:1 to 3:2 PE/EtOAc) to afford 5-(1-(3-bromobenzyl)-5-methyl-1H-1,2,4-triazol-3-yl)-3-(4-(trifluoromethoxy)phenyl)-1,2,4-oxadiazol as a white solid (53.6 g, 57.9%). ^{1}H NMR (600 MHz, $CDCl_3$) δ 8.28 (d, J = 8.8 Hz, 2H), 7.48 (d, J = 7.9 Hz, 1H), 7.41 (s, 1H), 7.34 (d, J = 8.8 Hz, 2H), 7.26 (d, J = 7.6 Hz, 1H), 7.17 (d, J = 7.9 Hz, 1H), 5.43 (s, 2H), 2.55 (s, 3H); ^{13}C NMR (126 MHz, DMSO-d_6) δ 168.9, 167.2, 155.4, 150.5, 148.2, 137.8, 131.0, 131.0, 130.5, 129.4, 126.9, 124.9, 121.9, 121.6, 119.9 (q, J = 258 Hz), 51.1, 11.6; ^{19}F NMR (471 MHz, DMSO-d_6) δ -56.6; HRMS (ESI$^+$) m/z: $[M+H]^+$ calcd. for $C_{19}H_{14}BrF_3N_5O_2$ 480.0277, 482.0257; found 480.0270, 480.0247.

Step 5: **Synthesis of IACS-010759** 5-(5-methyl-1-(3-(4-(methylsulfonyl)piperidin-1-yl)benzyl)-1H-1,2,4-triazol-3-yl)-3-(4-(trifluoromethoxy)phenyl)-1,2,4-oxadiazole

To a mixture of 5-(1-(3-bromobenzyl)-5-methyl-1H-1,2,4-triazol-3-yl)-3-(4-(trifluoromethoxy)phenyl)-1,2,4-oxadiazole (2.00 g, 4.16 mmol), 4-(methylsulfonyl)piperidine (1.02 mg, 6.24 mmol), and t-BuONa (800 mg, 8.33 mmol) in toluene (80 mL), 2-dicyclohexylphosphino-2',6'-di-i-propoxy-1,1'-biphenyl (580 mg, 1.25 mmol) and tris(dibenzylideneacetone)dipalladium (760 mg, 0.83 mmol) were added and the reaction mixture was degassed with argon for 3 mins, then heated to 140 ℃ for 18 hrs under argon atmosphere. The mixture was then cooled to RT, diluted with EtOAc (100 mL), filtered through a pad of celite, washed with EtOAc (100 mL) and concentrated under reduced pressure. The residue was purified by silica gel chromatography column (PE: EtOAc = 1:1 to pure EtOAc) to crude product, which was treated with EtOAc and Et_2O (v: v = 1:9, 30 mL). The resulting suspension was stirred at RT for 30 min, and then filtered to afford 5-(5-methyl-1-(3-(4-(methylsulfonyl)piperidin-1-yl)benzyl)-1H-1,2,4-triazol-3-yl)-3-(4-(trifluoromethoxy)phenyl)-1,2,4-oxadiazole as a white solid (905 mg, 39%). ^{1}H NMR (600 MHz, DMSO-d_6) δ 8.22 (d, J =

8.8 Hz, 2H), 7.61 (d, J = 8.2 Hz, 2H), 7.21 (t, *J* = 7.9 Hz, 1H), 6.97 (bs, 1H), 6.94 (dd, *J* = 8.3, 2.4 Hz, 1H), 6.64 (d, *J* = 7.5 Hz, 1H), 5.48 (s, 2H), 3.86 (bd, *J* = 13.4 Hz, 2H), 3.28 (m, 1H), 2.94 (s, 3H), 2.76 (m, 2H), 2.57 (s, 3H), 2.06 (bd, J = 13.4 Hz, 2H), 1.68 (ddd, *J* = 16.5, 12.5, 4.1 Hz, 2H); ^{13}C NMR (126 MHz, DMSO-d_6) δ 169.0, 167.2, 155.1, 150.7, 150.5, 147.9, 136.0, 129.6, 129.4, 124.9, 121.7, 119.9 (q, J = 258 Hz), 117.8, 115.5, 115.2, 58.6, 52.3, 47.2, 37.4, 23.7, 11.7; ^{19}F NMR (471 MHz, DMSO-d_6) δ -56.6; HRMS (ESI$^+$) m/z: $[M+H]^+$ calcd. for $C_{25}H_{26}F_3N_6O_4S$ 563.1683; found 563.1675.

Oxygen consumption

AML cells were suspended normal growth medium at a concentration of 1 x 10^7 cells/ml and 100 µl of cells were added to Seahorse 96-well plates pre-coated with Cell Tak. Plates were centrifuged and medium was replaced with pre-warmed (37^o C) 125 µl Seahorse medium (Seahorse XF medium with 2 mM glutamax, 10 mM glucose, 2 mM pyruvate) containing IACS-010759 or rotenone (41 nM). For AML cell lines, 3 x 10^5 total cells were seeded per well in Seahorse XF medium with 2 mM glutamine, 10 mM glucose, and 2 mM pyruvate. The mitostress test was performed with 1 oligomycin µM, 0.4-1 FCCP µM, and 1 antimycin µM. For oxygen consumption in permeabilized tumor cells (Fig. 1D), H460 cells were suspended in Seahorse XF assay medium and plated at a concentration of 15 x 10^3 cells/well of Seahorse 96-well plates pre-coated with Cell Tak. Plates were centrifuged and medium was replaced with pre-warmed (37º C) 100 µl of 10 mM pyruvate/ 2mM malate substrate + 4 µM FCCP (uncoupled) in the 1x Mitochondria Assay Solution (MAS) media. Immediately prior to IACS-010759 injection, Plasma Membrane Permeabilizer (PMP) was added to 1 nM and ADP was added to a final concentration of 4 nM. Final drug/substrate concentrations were: IACS-010759 10, 100 or 1000 nM; rotenone 100 nM; succinate 10 mM antimycin 4 µM. A detailed protocol is provided by Seahorse http://www.seahorsebio.com/resources/tech-writing/XF_PMP_Protocol.pdf.

Seahorse analyses for AML cell lines and the PDX model was performed according to Seahorse Biosciences protocol for the mitostress test. Briefly, 300,000 cells per well were seeded in 175 uL of Seahorse XF medium supplemented with 10 mM glucose, 2 mM glutamine, and 1 mM pyruvate. FCCP concentration was optimized for each cell line model (1.6-0.2 µM) and data was normalized to cell number.

Seahorse analyses for basal OCAR and ECAR were performed using reagents from Seahorse Bioscience as previously reported[48].

Ectopic expression of NDI-1

HEK293T cells were transfected with pCMV-dR8.9 packaging DNA vector, pMD2.G VSV-G-expressing envelope vector, and either pLenti6.3 NDI-1, pLenti6.3/V5 NDI-1, or pLenti6.3/V5 GFP plasmid DNA. 2 x 10^5 H460 cells were transduced in a 6-well plate with 2 ml of viral supernatant supplemented with polybrene to a final concentration of 8 µg/ml. After infection, transduced cells were selected by growing in 7 µg/ml blastacidin. The concentration of IACS-010759 used in the graph in Fig. 1e was 14 nM.

Isolated mouse complex I assay.

Complex I was isolated from mouse heart mitochondria using an adaptation of the method of Sharpley and coworkers [49]. The concentration of IACS-010759 in Fig. 1f was 60 nM. The NADH:decylubiquinone assay is described in Sharpley et al. [49] and the $APAD^+$ and H_2O_2 assays are described in Birrell et al. [50].

Generation of clonal cell lines resistant to IACS-010759

H292 cells ($1x10^6$ cells/plate) were seeded in 15 cm dishes in galactose growth medium and treated with 1 nM IACS-010759 (IC_{65}) 1 nM IACS-010759 for 3 weeks, followed by exposure to 8 nM IACS-010759 (IC_{95}) until resistant clones emerged. Twenty-six resistant clones were isolated from 4 independent experiments were seeded at $5x10^3$ cells/well in 96-well plates in 100 µl galactose growth medium. After cells became fully attached, IACS-010759 or rotenone was added to final concentrations of 370 nM-18 pM for 3 days. Plates were scanned in in IncuCyte® live-cell analysis system prior to analysis via Hoechst and PI. Subsequently, both Hoechst and PI using an Operetta high-content imaging system.RNAseq was conducted on the parental line and 12 resistant clones, uncovering a single non-synonymous, heteroplasmic (35% to 50%), recurrent mutation in the mitochondrial-encoded gene MT-ND1 in 9 of the 12 resistant clones that conferred the following amino-acid change: L>55F (T>3469C). Paired-end reads were initially aligned to transcript sequences of complex I genes with Bowtie 2 [51] and the aligned fragments were probabilistically assigned to transcripts using eXpress [52]. Variants from the reference genome were called using the mpileup command in SAMtools. MutPred [53] analysis of the L>55F variant classifies the alteration as potentially pathogenic (MutPred score = 0.8); this alteration is found at a very low frequency in mtDNA sequences in Genebank (1:30589 based on full-length mitochondrial genomes deposited in Genebank prior to October 28th, 2015), suggesting it is unlikely to be a polymorphism. The mutation was confirmed in four of the resistant clones by cloning the MT-ND1 gene sequence (ZERO blunt PCR [Invitrogen]) and analyzing purified plasmid DNA via Sanger sequencing using the following primers: *Forward*: GTAAAACGACGGCCAGT and *Reverse*: AACAGCTATGACCATG.

Metabolomics for glycolysis deficient models

NB-1, D423, Gli56, A1207, SW1088 and U87 were plated and treated with DMSO or 100 nM IACS-010759 in 10-cm plate with adjusted density in the goal to reach similar density at the time of harvesting. Two days after, the cells were briefly washed in cold PBS, scrapped in 80% methanol, and spun down. The supernatant was dried in a GeneVac HT4 using the low temperature program (SP Scientific). The dried samples were resuspended and subjected to LC-MS analysis that covers over 200 metabolites at Dr John M Asara's group at Beth Israel Deaconess Medical Center, as previously described [54]. Analysis of metabolite peak area integrated total ion chromatogram values was carried out in R. Metabolites with missing data in any sample were excluded, and the remaining values were quantile normalized. Statistical comparisons of groups was performed with limma, and all p-values reported were corrected for multiple hypothesis testing by the Benjamini and Hochberg method.

LC-MS for targeted metabolomics and stable-isotope tracing in AML cell lines

For targeted metabolomics, dried cellular extracts from OCI-AML3 cultures were reconstituted with 1:1 acetonitrile:water (40 uL) and aliquots (5 uL) were analyzed on an Agilent 1290 ultra-

high performance liquid chromatography (UHPLC) system coupled with an Agilent 6550 quadrupole-time of flight (Q-TOF) mass spectrometer operating in negative ion mode. Details about LC-MS analysis conditions are reported in Appendix I. Acquired Q-TOF raw data was processed using Agilent MassHunter Profinder 8.0 software and target metabolites were identified using the built-in batch targeted feature extraction algorithm which utilized an in-house accurate mass-retention time (AMRT) database library including 126 endogenous metabolites. Identified compound signal intensities were extracted and subjected to statistical analysis in Agilent Mass Profiler Professional (MPP). Sample metabolite raw abundancies were log2 transformed, normalized by their correspondent sample protein content or viable cell count and centered to their median signal intensities. The unpaired Welch's t-test was used to determine statistically significant variations across sample groups (For detailed methodology refer to Appendix I).

For stable-isotope tracing experiments, samples for LC-MS analysis were prepared as described above and analyzed on an Agilent 6550 Q-TOF. The raw data was analyzed in MassHunter Profinder 8.0 by running the batch isotopologue extraction algorithm against an AMRT in-house compound library including the compounds of interest. The resulting isotopologue abundancies were corrected for their isotopic natural abundance, extracted as detailed CVS files, and tested for significant variations using a Welch's t-test. Details about cell growth and LC-MS analysis are reported in Appendix I (For detailed methodology refer to Appendix I).

Primary AML cells and normal bone marrow

Peripheral blood samples from patients with AML were collected during routine diagnostic procedures after informed consent was obtained in accordance with the regulations and protocols (LAB 01-473) approved by the MDACC Investigational Review Board (IRB) in accordance with IRB regulations of The University of Texas MD Anderson Cancer Center and the Declaration of Helsinki. AML samples were analyzed under the Investigational Review Board-approved laboratory protocol PA13-1025. Briefly, mononuclear cells were separated by Ficoll-Hypaque density gradient centrifugation and incubated in RBC lysis buffer (ammonium chloride solution) to remove red blood cells. Primary leukemia samples were maintained in StemEZ Serum-Free Medium. Viability and induction of apoptosis were assessed simultaneously using flow cytometry. 1-3 million cells were grown in triplicate in 24-well plates and exposed to DMSO or IACS-010759. Cells were harvested after 3, 4 or 5 days of exposure to agent and resuspended in binding buffer containing Annexin V. Apoptotic cells were detected by Annexin V flow cytometry after gating on CD45+ leukemic cells. Viable cells were detected by flow cytometry with anti–human CD45-FITC antibody (BD Pharmingen) staining after exclusion of nonviable cells by diamidino-2-phenylindole (DAPI; Sigma-Aldrich) and apoptotic cells. Flow Cytometry was performed on Gallios Flow Cytometer and data analyzed using Kaluza Flow Analysis software (Beckman Coulter). For normal bone marrow, the same procedure was followed.

Gene expression signature

To determine whether specific gene pathways were altered by treatment with IACS-010759, REACTOME pathway analysis was performed on the genes that were significantly up-regulated

(132 genes) or down-regulated (132 genes) in >2 cell lines by 24-hour treatment with 100 nM IACS-010759. The top four gene pathways upregulated in response to IACS-010759 were all related to amino acid biosynthesis (Supplementary Fig. 13a), consistent with the findings described above that metabolite levels are altered in response to IACS-010759. The fifth pathway up-regulated included genes regulated by *ATF4*, which is a transcription factor that upregulates genes that that deal with cellular stress in response to decreased amino acids and energy intermediates. The top 5 down-regulated pathways all involve genes involved in cell cycle progression (Supplementary Fig. 13b).

Genes whose expression was modulated by treatment with IACS-010759 in >3 cell lines were selected for validation *in vivo* with a custom NanoString codeset. Samples from an acute PK/PD study conducted in a primary patient-derived AML mouse xenograft model were harvested in triplicate after 48 hours of treatment with 1, 2.5, and 7.5 mg/kg IACS-010759 and in duplicate for the vehicle. Analysis of NanoString data was carried out using the statistical computing language R. Normalization factors were calculated based on the internal positive controls and a selected set of housekeeping genes (*CLTC, TBP, ALAS1, ACTB*, and *RPL19*) according to the nCounter Expression Data Analysis Guide. For each sample, to control for variability in hybridization across samples, the geometric mean of the internal controls is calculated and then used to normalize across samples. To control for variability associated with the amount of input mRNA, the geometric mean of the housekeeping genes is calculated and then used to normalize samples for the amount of input mRNA. Data were normalized to vehicle samples, and genes ranked by the magnitude of alteration at the highest dose (Supplementary Fig. 8c). A subset of genes were dose-dependently downregulated upon treatment, with > 2 fold decrease in expression at the highest dose of IACS-010759 (Supplementary Fig. 13c, d,e). Variability in mRNA signal for each gene was minimal across the three mice within a dosing group.

The top scoring gene was IL8 and it was equally inhibited at all three dose levels (Supplementary Figs. 13d,e). In contrast, other genes showed a dose-dependent inhibition over this range (Supplementary Figs. 13d,e). A 'summary score' was constructed based on the average fold change of the 12 genes for which the highest dose-dependent downregulation was observed in response to IACS-010759 (*RRM2, HMGN2, DHCR24, PCNA, KIF11, TK1, KLGAP25, KIF20A, CDCA5, CCNB1* and *FEN1*) and plotted *vs.* plasma levels for the PK/PD analysis shown in Supplementary Fig. 13f.

This analysis shows a dose-dependent decrease in expression of this group of genes in response to IACS-010759 treatment.

Life Sciences Reporting Summary

Additional details on experimental details and design are available in the Life Sciences Report Summary.

References (Methods Only):

48 Sun, Y. *et al.* Metabolic and transcriptional profiling reveals pyruvate dehydrogenase kinase 4 as a mediator of epithelial-mesenchymal transition and drug resistance in tumor cells. *Cancer Metab* **2**, 20, doi:10.1186/2049-3002-2-20 (2014).

49 Sharpley, M. S., Shannon, R. J., Draghi, F. & Hirst, J. Interactions between phospholipids and NADH:ubiquinone oxidoreductase (complex I) from bovine mitochondria. *Biochemistry* **45**, 241-248, doi:10.1021/bi051809x (2006).

50 Birrell, J. A., Yakovlev, G. & Hirst, J. Reactions of the flavin mononucleotide in complex I: a combined mechanism describes NADH oxidation coupled to the reduction of APAD+, ferricyanide, or molecular oxygen. *Biochemistry* **48**, 12005-12013, doi:10.1021/bi901706w (2009).

51 Langmead, B. & Salzberg, S. L. Fast gapped-read alignment with Bowtie 2. *Nat Methods* **9**, 357-359, doi:10.1038/nmeth.1923 (2012).

52 Roberts, A. & Pachter, L. Streaming fragment assignment for real-time analysis of sequencing experiments. *Nat Methods* **10**, 71-73, doi:10.1038/nmeth.2251 (2013).

53 Li, B. *et al.* Automated inference of molecular mechanisms of disease from amino acid substitutions. *Bioinformatics* **25**, 2744-2750, doi:10.1093/bioinformatics/btp528 (2009).

54 Yuan, M., Breitkopf, S. B., Yang, X. & Asara, J. M. A positive/negative ion-switching, targeted mass spectrometry-based metabolomics platform for bodily fluids, cells, and fresh and fixed tissue. *Nat Protoc* **7**, 872-881, doi:10.1038/nprot.2012.024 (2012).

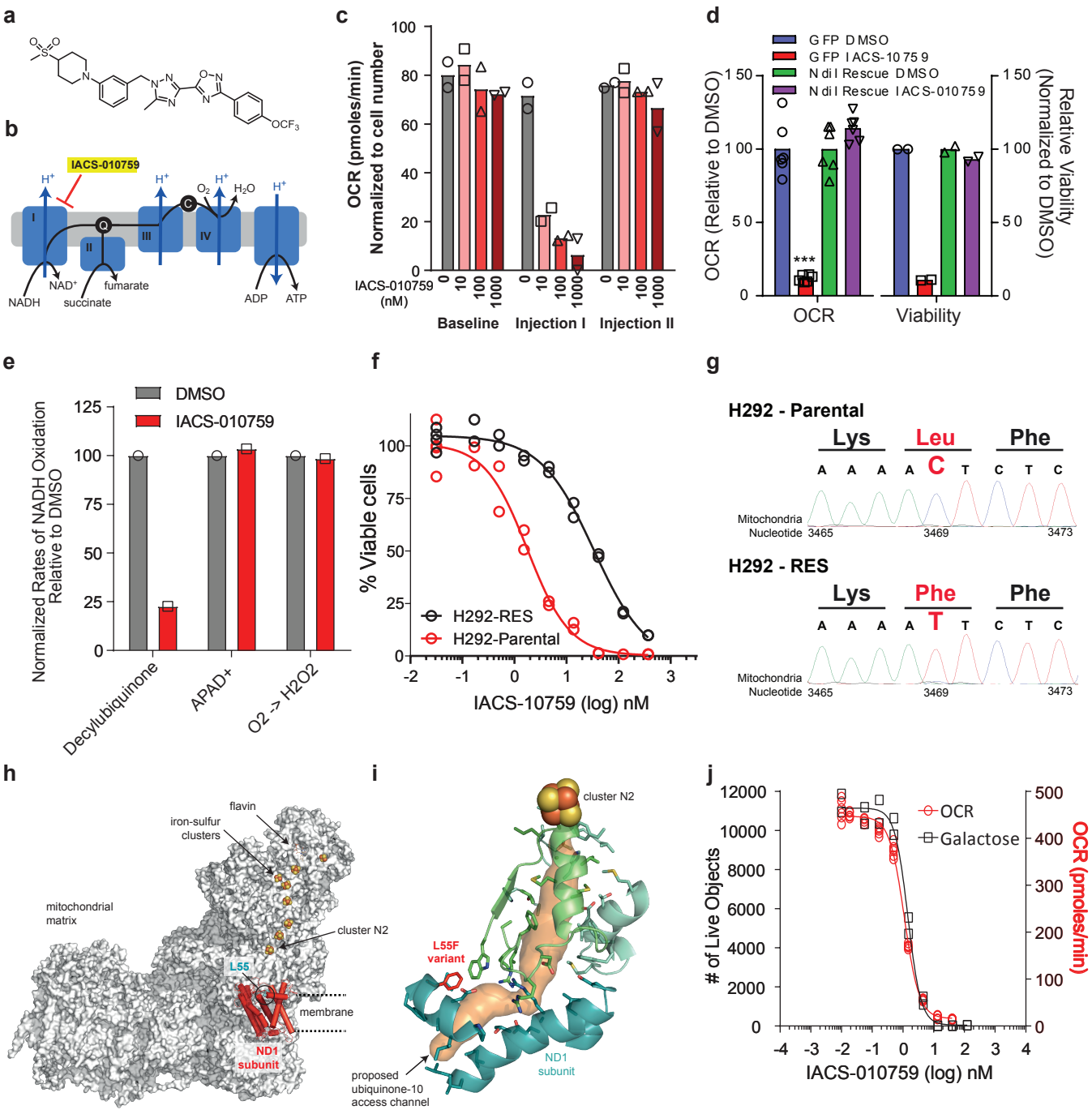
a
b
IACS-010759
H+
O2
H2O
NADH
NAD+
succinate
fumarate
ADP
ATP
c
OCR (pmoles/min)
Normalized to cell number
IACS-010759 (nM)
Baseline
Injection I
Injection II
d
GFP DMSO
GFP IACS-10759
Ndi1 Rescue DMSO
Ndi1 Rescue IACS-010759
OCR (Relative to DMSO)
Relative Viability (Normalized to DMSO)
***
OCR
Viability
e
DMSO
IACS-010759
Normalized Rates of NADH Oxidation Relative to DMSO
Decylubiquinone
APAD+
O2 -> H2O2
f
% Viable cells
H292-RES
H292-Parental
IACS-10759 (log) nM
g
H292 - Parental
Lys
Leu
Phe
Mitochondria Nucleotide
3465
3469
3473
H292 - RES
Phe
h
flavin
iron-sulfur clusters
mitochondrial matrix
cluster N2
L55
membrane
ND1 subunit
i
cluster N2
L55F variant
ND1 subunit
proposed ubiquinone-10 access channel
j
# of Live Objects
OCR
Galactose
OCR (pmoles/min)
IACS-010759 (log) nM

Figure 1

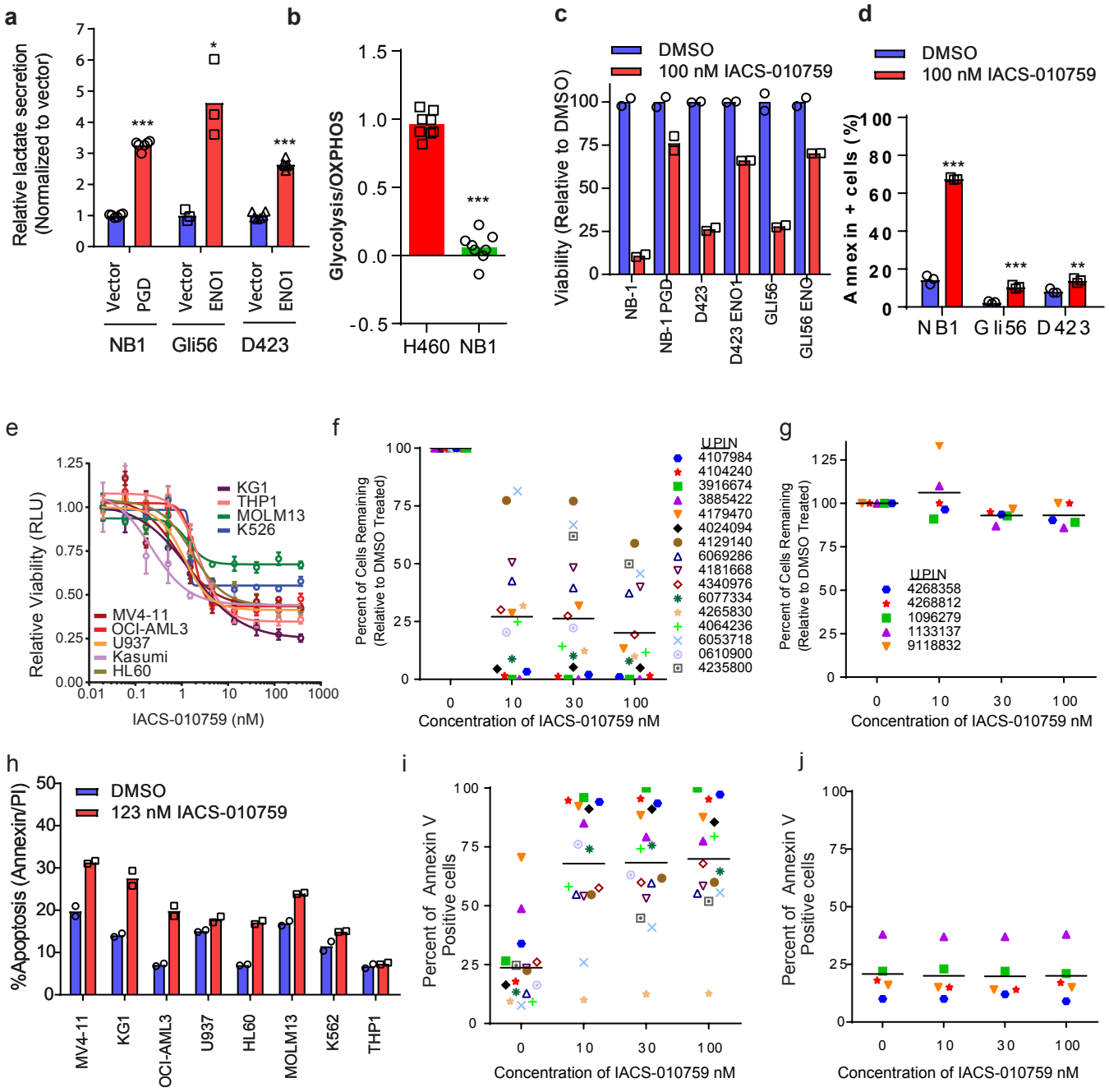
a
Relative lactate secretion (Normalized to vector)
Vector
PGD
Vector
ENO1
Vector
ENO1
NB1
Gli56
D423
b
Glycolysis/OXPHOS
H460
NB1
c
DMSO
100 nM IACS-010759
Viability (Relative to DMSO)
NB-1
NB-1 PGD
D423
D423 ENO1
GLI56
GLI56 ENO
d
DMSO
100 nM IACS-010759
Annexin + cells (%)
NB1
Gli56
D423
e
Relative Viability (RLU)
KG1
THP1
MOLM13
K526
MV4-11
OCI-AML3
U937
Kasumi
HL60
IACS-010759 (nM)
f
Percent of Cells Remaining (Relative to DMSO Treated)
UPN
4107984
4104240
3916674
3885422
4179470
4024094
4129140
6069286
4181668
4340976
6077334
4265830
4064236
6053718
0610900
4235800
Concentration of IACS-010759 nM
g
Percent of Cells Remaining (Relative to DMSO Treated)
UPN
4268358
4268812
1096279
1133137
9118832
Concentration of IACS-010759 nM
h
%Apoptosis (Annexin/PI)
DMSO
123 nM IACS-010759
MV4-11
KG1
OCI-AML3
U937
HL60
MOLM13
K562
THP1
i
Percent of Annexin V Positive cells
Concentration of IACS-010759 nM
j
Percent of Annexin V Positive cells
Concentration of IACS-010759 nM

Figure 2

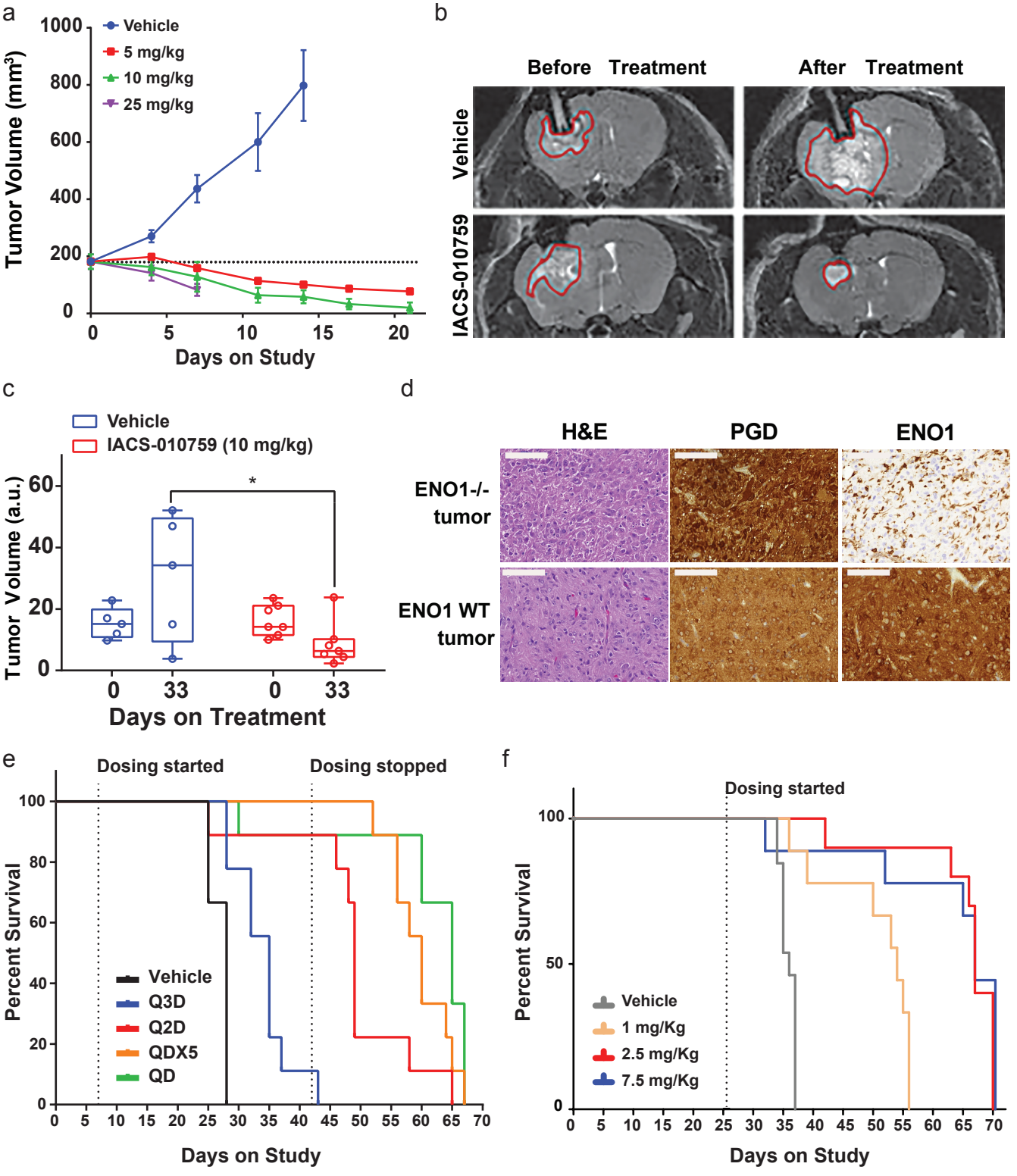

Lorem ipsum

Figure 3

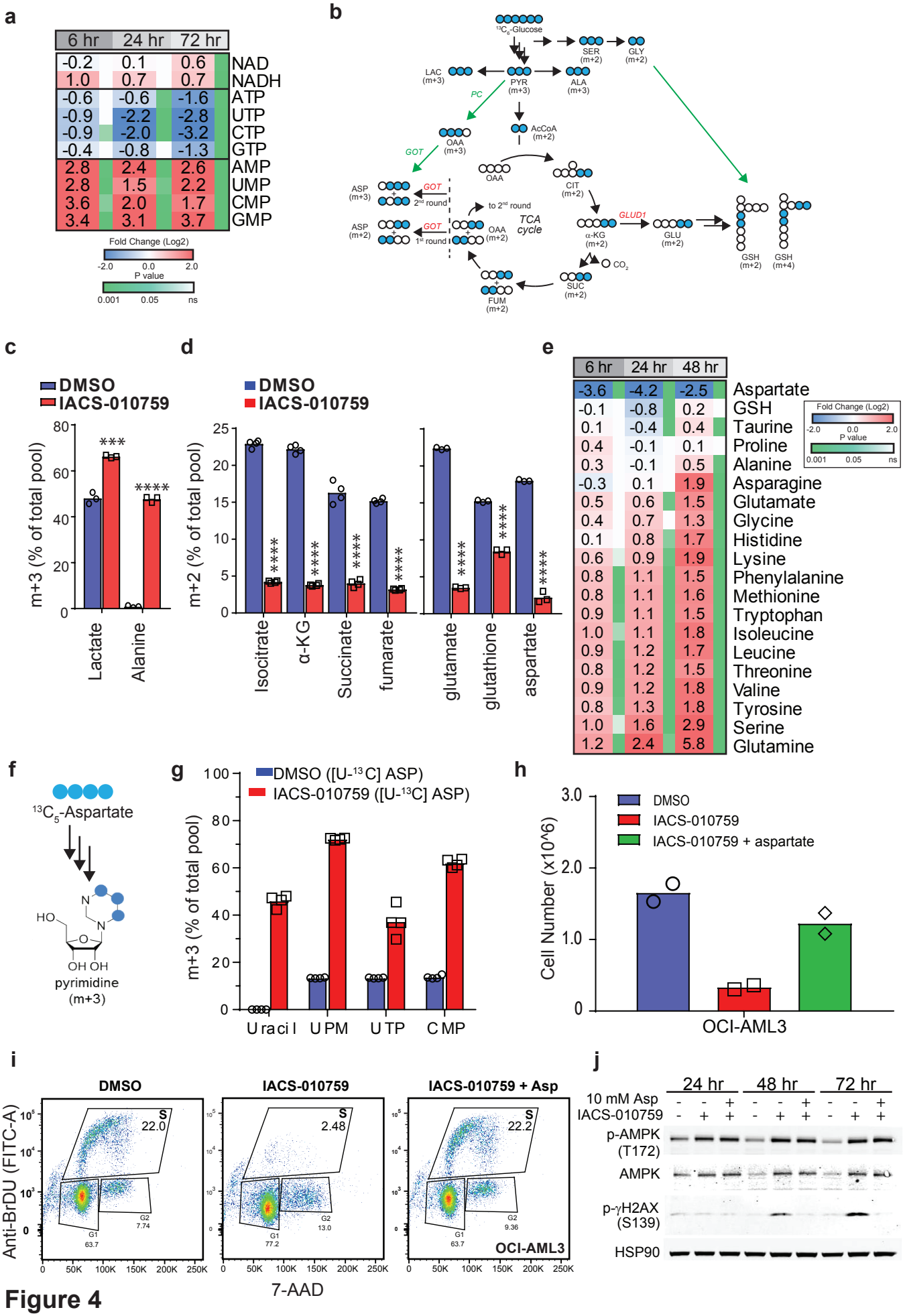
a
6 hr
24 hr
72 hr
-0.2
0.1
0.6
NAD
1.0
0.7
0.7
NADH
-0.6
-0.6
-1.6
ATP
-0.9
-2.2
-2.8
UTP
-0.9
-2.0
-3.2
CTP
-0.4
-0.8
-1.3
GTP
2.8
2.4
2.6
AMP
2.8
1.5
2.2
UMP
3.6
2.0
1.7
CMP
3.4
3.1
3.7
GMP
Fold Change (Log2)
-2.0
0.0
2.0
P value
0.001
0.05
ns
b
13C6-Glucose
SER (m+2)
GLY (m+2)
LAC (m+3)
PYR (m+3)
ALA (m+3)
PC
AcCoA (m+2)
OAA (m+3)
GOT
OAA
CIT (m+2)
ASP (m+3)
GOT
2nd round
to 2nd round
ASP (m+2)
GOT
1st round
OAA (m+2)
TCA cycle
GLUD1
α-KG (m+2)
GLU (m+2)
GSH (m+2)
GSH (m+4)
CO2
SUC (m+2)
FUM (m+2)
c
DMSO
IACS-010759
m+3 (% of total pool)
***
****
Lactate
Alanine
d
DMSO
IACS-010759
m+2 (% of total pool)
****
Isocitrate
α-KG
Succinate
fumarate
glutamate
glutathione
aspartate
e
6 hr
24 hr
48 hr
-3.6
-4.2
-2.5
Aspartate
-0.1
-0.8
0.2
GSH
0.1
-0.4
0.4
Taurine
0.4
-0.1
0.1
Proline
0.3
-0.1
0.5
Alanine
-0.3
0.1
1.9
Asparagine
0.5
0.6
1.5
Glutamate
0.4
0.7
1.3
Glycine
0.1
0.8
1.7
Histidine
0.6
0.9
1.9
Lysine
0.8
1.1
1.5
Phenylalanine
0.8
1.1
1.6
Methionine
0.9
1.1
1.5
Tryptophan
1.0
1.1
1.8
Isoleucine
0.9
1.2
1.7
Leucine
0.8
1.2
1.5
Threonine
0.9
1.2
1.8
Valine
0.8
1.3
1.8
Tyrosine
1.0
1.6
2.9
Serine
1.2
2.4
5.8
Glutamine
Fold Change (Log2)
-2.0
0.0
2.0
P value
0.001
0.05
ns
f
13C5-Aspartate
HO
N
N
O
OH OH
pyrimidine
(m+3)
g
DMSO ([U-13C] ASP)
IACS-010759 ([U-13C] ASP)
m+3 (% of total pool)
Uracil
UPM
UTP
CMP
h
DMSO
IACS-010759
IACS-010759 + aspartate
Cell Number (x10^6)
OCI-AML3
i
DMSO
IACS-010759
IACS-010759 + Asp
Anti-BrDU (FITC-A)
S
22.0
G2
7.74
G1
63.7
S
2.48
G2
13.0
G1
77.2
S
22.2
G2
9.36
G1
63.7
OCI-AML3
7-AAD
j
24 hr
48 hr
72 hr
10 mM Asp
IACS-010759
p-AMPK (T172)
AMPK
p-γH2AX (S139)
HSP90

Figure 4

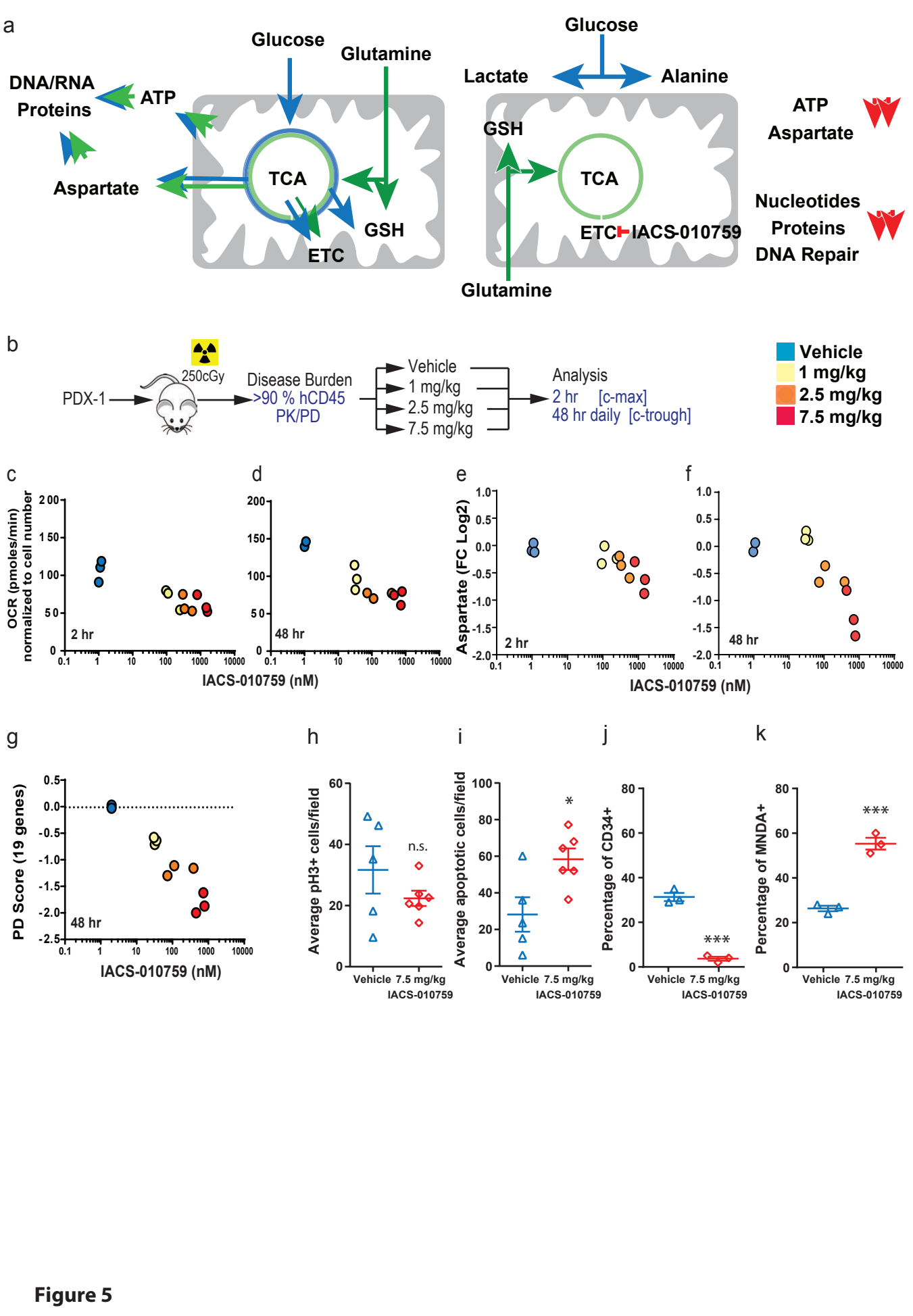
a
Glucose
Glutamine
DNA/RNA
Proteins
ATP
Aspartate
TCA
GSH
ETC
Glucose
Lactate
Alanine
GSH
TCA
ETC
IACS-010759
Glutamine
ATP
Aspartate
Nucleotides
Proteins
DNA Repair
b
PDX-1
250cGy
Disease Burden
>90 % hCD45
PK/PD
Vehicle
1 mg/kg
2.5 mg/kg
7.5 mg/kg
Analysis
2 hr [c-max]
48 hr daily [c-trough]
Vehicle
1 mg/kg
2.5 mg/kg
7.5 mg/kg
c
OCR (pmoles/min)
normalized to cell number
2 hr
IACS-010759 (nM)
d
48 hr
e
Aspartate (FC Log2)
2 hr
IACS-010759 (nM)
f
48 hr
g
PD Score (19 genes)
48 hr
IACS-010759 (nM)
h
Average pH3+ cells/field
n.s.
Vehicle
7.5 mg/kg
IACS-010759
i
Average apoptotic cells/field
*
Vehicle
7.5 mg/kg
IACS-010759
j
Percentage of CD34+
***
Vehicle
7.5 mg/kg
IACS-010759
k
Percentage of MNDA+
***
Vehicle
7.5 mg/kg
IACS-010759

Figure 5